NACA

RESEARCH MEMORANDUM

DRAG AND ROLLING-MOMENT EFFECTIVENESS OF TRAILING-EDGE SPOILERS AT MACH NUMBERS 2.2 AND 5.0

By Thomas N. Canning and Charles E. DeRose

Ames Aeronautical Laboratory
Moffett Field, Calif.

NATIONAL ADVISORY COMMITTEE
FOR AERONAUTICS

WASHINGTON

October 3, 1955

NATIONAL ADVISORY COMMITTEE FOR AERONAUTICS

RESEARCH MEMORANDUM

DRAG AND ROLLING-MOMENT EFFECTIVENESS OF TRAILING-EDGE SPOILERS AT MACH NUMBERS 2.2 AND 5.0

By Thomas N. Canning and Charles E. DeRose

SUMMARY

Free-flight measurements were made of the rolling effectiveness and drag of trailing-edge spoilers on low-aspect-ratio wings with both laminar and turbulent boundary layers at Mach numbers of 2.2 and 5.0. Reynolds numbers for the rolling-effectiveness tests were from 1.15 million to 1.50 million while drag results were obtained for Reynolds numbers of from 0.24 million to 3.50 million based on wing chord.

As found previously, the effect of a spoiler deflected from the surface of a wing is to cause boundary-layer separation upstream. A region of entrapped air is formed between the separation point and the forward face of the spoiler. In section view the flow at supersonic speeds looks somewhat like that produced by a wedge with its leading edge at the separation point and its trailing edge along the top of the spoiler. This simplified model of the flow is useful in estimating the effectiveness of the spoiler. The normal force and drag of the spoiler are roughly equal to that of a split flap deflected 15° and of such a chord as to place the trailing edge at the top of the spoiler.

The present data show that a change from laminar to turbulent boundary layer on the wing ahead of the separation point affects the rolling moments by increasing the angle of flow deflection and decreasing the chordwise area for wing-tip leakage. At $M = 5.0$, these effects made the rolling moment with turbulent flow 35 percent greater than with laminar flow. At $M = 2.2$, this difference was not shown conclusively. Wing-tip fences, added to eliminate wing-tip leakage, produced a 20-percent increase in rolling-moment coefficient over that for the plain turbulent-separation case at $M = 5.0$ and a somewhat smaller increase at $M = 2.2$.

In the case of turbulent boundary-layer flow the drag rise of spoilers, based on exposed spoiler area, was found to be independent of both spoiler height and Reynolds number at both Mach numbers. For laminar flow ahead of the separation point, the drag coefficient was generally lower than that measured for turbulent flow and varied with the ratio of spoiler

height to boundary-layer thickness. At both Mach numbers, the laminar-flow drag coefficient was equal to the turbulent-flow value at the highest spoiler deflection.

INTRODUCTION

One serious problem in developing useful guided missiles lies in providing adequate servo power to overcome the aerodynamic and inertial hinge moments of the controls. The weight of the internal hardware, servo motors, amplifiers, accumulators, etc., is fixed largely by the hinge moments to be overcome. Spoilers, because of their small actuating-force requirements, appear advantageous for those missile applications where they can supply sufficient control.

Information on the performance of spoilers at supersonic speeds is given in references 1, 2, 3, 4, and 5. These references give detailed information on the normal-force development of trailing-edge spoilers applied to wings of various plan forms and sweep at Mach numbers below 2.6. In general, these references show that the spoilers develop normal force comparable to that produced by flap-type controls on airplane-type wings at Mach numbers below 2.6. It is the intent of this investigation to extend the existing data on trailing-edge spoilers in two respects: (1) to investigate the control effectiveness of spoilers on aspect-ratio-1 missile-type wings in the Mach number range from 2.2 to 5.0, and (2) to measure the drag penalty of spoiler deflection with both laminar and turbulent flow.

The capabilities of a spoiler as the primary control surface of a canard air-to-air missile and an application of spoilers as unbalancing servotabs to eliminate aerodynamic hinge moments on an all-movable control are discussed in an appendix.

SYMBOLS

A frontal area of cross section of ring spoiler model, sq ft

a frontal area of spoiler, sq ft

b wing span, ft

C_D drag coefficient, $\frac{\text{drag force}}{Aq}$

ΔC_D drag-rise coefficient, $\frac{\text{spoiler drag force}}{aq}$

C_h hinge-moment coefficient at control shaft, $\frac{\text{hinge moment}}{qSc}$

C_l rolling-moment coefficient, $\frac{\text{rolling moment}}{qSb}$

C_{l_p} damping-in-roll coefficient, $\frac{dC_l}{d\frac{pb}{2V}}$

C_m pitching-moment coefficient, $\frac{\text{pitching moment}}{qSc}$

c wing chord, ft

d body diameter, ft

e error, $\delta - \delta_i$, deg

f frequency of pitching oscillation, cps

h spoiler height, ft

k constant

I_x rolling moment of inertia of model, slug-ft^2

I_h effective moment of inertia of all-movable wing about hinge line

L_δ rolling moment due to spoiler deflection, ft-lb

L_p rolling moment due to rolling velocity, ft-lb

M Mach number

ΔP pressure increment above ambient pressure, lb/sq ft

p rolling velocity, radians/sec

q dynamic pressure, lb/sq ft

R Reynolds number based on free-stream properties and wing-chord length

S total exposed area of wing panels, sq ft

t time, sec

V velocity of model with respect to air stream, ft/sec

α angle of attack, radians

δ deflection angle, deg

δ_i desired deflection angle, deg

ρ air density, slugs/cu ft

φ roll angle, deg

Subscript

o conditions at $t = o$

FACILITIES AND TECHNIQUES

Wind Tunnel

The tests which are the subject of this report were conducted in the Ames supersonic free-flight wind tunnel. This facility is a short ballistic range inside a variable pressure, supersonic, blowdown wind tunnel. In this tunnel, models are fired upstream through the 15-foot-long test section (from a gun located in the diffuser) in order to obtain data at Mach numbers above 3. For lower speeds, the models are fired through still air. The aerodynamic data are obtained from time histories of the model motion as recorded by four shadowgraph stations, a chronograph, and a high-speed motion-picture camera. Details of tunnel operation are given in reference 6.

Models

All of the models used in this study were fired from a rifled 37-mm cannon. Two sets of models were used in this investigation; the first was used for measuring the spoiler-aileron effectiveness, and the second for measuring the drag increment resulting from spoiler deflection.

The first set of models had cone-cylinder bodies of revolution fitted with cruciform, rectangular wings having an aspect ratio of 1. Dimensions of these models are given in figure 1. The model bodies were made of aluminum and magnesium. The nose was ballasted with brass and the base drilled with lightening holes to give a stable center-of-gravity position. The wings were steel and were continuous through the body in order to promote stiffness. Spoilers, made of steel, were pinned and brazed to the wing trailing edges. Spoiler-aileron deflections of 0, 0.02c, 0.04c, and

0.08c were tested on the basic configuration; typical models are shown in figure 2. Modifications to the standard models consisted of polishing the wing surfaces or cutting saw-tooth notches in the leading edges to promote laminar or turbulent flow; wing-tip fences were also mounted on several models to evaluate tip-loss effects. A modified model with 0.08c spoiler height, saw-tooth leading edge, and wing-tip fences is shown in figure 2(b). Most of the above modifications were tested on the $h/c = 0.08c$ models.

The models used for measuring profile drag were of the type shown in figure 3 - thin-walled tubes flown with their axes parallel to the stream. These models, which will be referred to as ring models, were machined from solid bar stock. In order to control the deceleration in the wind-tunnel test section, aluminum was used for the low-drag configurations and steel for those having high drag. Laminar flow was promoted by polishing the surface of some models and turbulent flow was induced on others by tripping the boundary layer with fine screw threads near the leading edge.

All the ring models that were expected to have transition occurring ahead of the spoiler, whether the flow ahead of separation was laminar or turbulent, were equipped with boundary-layer trips near the leading edge on the inside surface. This assured turbulent flow on both sides of the trailing edge and made it simpler to estimate the base drag.

Both sets of models were fired from a rifled 37-mm gun. A complete assembly of model and support for launching is shown in figure 4 for the aileron model, and in figure 5 for the ring model. The aileron models were keyed to the sabot to provide a positive drive for spinning and to prevent the wings from rotating into the fingers. The ring models relied on friction drive for their rotation.

TESTING TECHNIQUES

Rolling Moment

In the rolling-moment tests, a high-speed motion-picture camera was used to photograph a nearly head-on view of the model silhouetted against the reflector of a large searchlight. The film in this camera moves steadily, instead of intermittently, and the image is traversed with the film. The history of roll position along with timing marks made on the film by an argon lamp flashing at a controlled frequency permitted determination of rolling acceleration due to aileron deflection. The arrangement of equipment used for the present test is shown in figure 6.

The models were launched with the spoilers deflected to produce roll opposite to that imparted by the rifling of the gun. The gun was so positioned in the wind-tunnel diffuser that the model, decelerating in roll

under the combined effects of damping in roll and spoiler deflection, reached zero or a very small roll rate in the center of the test section. This firing plan was used to keep the rolling moment due to rolling very small during the time data were obtained.

A portion of a typical film record showing successive frames and timing marks is given in figure 7. In this figure, it is possible to see even such fine details as the wing-tip fences. In this particular film record, the model has just reversed roll direction and has a counterclockwise roll velocity of about 2° per frame or 170 radians per second (wing-tip helix angle = 0.004 radian). A sample roll position versus time record is given in figure 8 which shows very clearly this reversal of roll direction.

The net rolling moment acting on the model is given by

$$L_{\delta} - L_p = \ddot{\varphi} I_x \tag{1}$$

If the rolling moment due to rolling is kept small with respect to the moment due to spoiler deflection, the total moment acting on the model can be assumed constant since L_{δ} is constant and L_p varies only slightly. Thus

$$\ddot{\varphi} = \frac{L_{\delta} - L_p}{I_x} = \text{constant} \tag{2}$$

Integrating twice gives the equation for roll position as a function of time.

$$\varphi = \varphi_o + \dot{\varphi}_o t + \frac{1}{2} \ddot{\varphi}_o t^2 \tag{3}$$

The data obtained are fitted to equation (3) by a least-squares procedure to obtain the constants φ_o, $\dot{\varphi}_o$, and $\ddot{\varphi}_o$ which are the values of roll position, velocity, and acceleration at the center of the length of the test section. From $\ddot{\varphi}_o$, the value of $L_{\delta} - L_p$ is obtained from equation (2). The rolling moment due to rolling, L_p, is calculated from the average value of the rolling velocity, $\dot{\varphi}_o$. This value of L_p was usually less than 10 percent of L_{δ} and in no case did it exceed 25 percent of L_{δ}. At $M = 2.2$, damping in roll was measured experimentally for $h/c = 0$ in order to evaluate L_p for the other configurations. The theoretical value of damping in roll given by reference 7 was used at $M = 5.0$ because it was not possible to obtain a value of C_{l_p} experimentally. The use of theory here was believed justifiable because of the small size of the damping-in-roll corrections.

Drag

Drag of the models was determined by measuring axial deceleration. The shadowgraph-chronograph equipment described in reference 6 was used. The change in profile drag due to deflecting the spoilers was obtained by measuring the difference in drag between a test model with a spoiler and a tare model without one. This experimental difference in drag was corrected for small differences in model geometry and test conditions.

Accuracy

For the rolling-moment tests, imperfect fin alinement is the greatest potential source of error. However, to minimize errors from this source, all fins were checked with a dial indicator prior to test and were straightened to within 0.001 inch in a chord length of 0.840 inch. An additive error in fin alinement of 0.001 inch on all four fins would introduce a 10-percent error in C_l for $h/c = 0.02c$ at $M = 2.2$ and about an 18-percent error at $M = 5.0$ for the same spoiler height. As h/c increases, the percent error in C_l decreases. These values of 10-percent and 18-percent possible error are an absolute maximum and it is believed that the real error from this source is of the order of 5 percent since the misalinement was never systematic and was usually below the value of 0.001 inch.

Another source of error arises from the fact that the models in free flight experience small oscillations in both pitch and yaw, usually less than 6°. This error, however, is believed to be small since there was no correlation between measured rolling moment and amplitude of pitching oscillation.

The probable random errors in measurement of test conditions and model dimensions are listed below.

$V = 0.5$ percent
$b = 0.1$ percent
$d = 0.1$ percent
$t = 0.2$ percent
$S = 0.05$ percent
$I_X = 0.5$ percent
$\varphi = 0.010$ radians

In view of the above estimations, it is felt that the rolling-moment coefficients are correct within ±6 percent at $h/c = 0.02$.

In the case of the drag measurements, there are no known systematic errors of consequence. The deceleration of the ring models was sufficiently

great to allow accurate measurement of drag. The probable random errors in measurement of model dimensions are comparable with those listed for the rolling-moment tests. The measurements of total drag had a scatter of ±2 percent. Since the incremental spoiler drag coefficients are obtained as a difference between two experimental values, the error is amplified. For spoilers larger than 0.02c, the incremental drag data are thought to be correct to within ±6 percent.

RESULTS AND DISCUSSION

Rolling Effectiveness

The variation of C_l with spoiler deflection is plotted for $M = 5.0$ and $M = 2.2$ in figure 9 for models having wings of three different degrees of surface smoothness. The data for $M = 5.0$ (fig. 9(a)) appear to be strongly influenced by the surface roughness of the wings. The higher effectiveness points were obtained from models with saw-tooth wing leading edges and with some unmodified models. Lower effectiveness was noted for models having polished wings with smooth leading edges. Some unmodified models also exhibited this reduced effectiveness. The effectiveness of the spoilers approaches that expected of the hypothetical, variable-chord split flap up to $0.04c$ deflection. A reduced effectiveness is shown by polished models at large spoiler deflections.

The saw-tooth wing leading edges have proven, in previous tests, to produce fully turbulent boundary layers under the conditions of the present test. That the boundary layer remained laminar to the separation point on the polished wings was less easily determined. Observations of the wing-tip-leakage flow in the latter case show a brief run without eddies, followed by transition and turbulent flow ahead of the spoiler (see fig. 10(a)). In the absence of other evidence, this flow pattern was assumed to indicate laminar flow over the entire wing surface ahead of the separation point. The contrast between this flow pattern and that with saw-tooth leading edge is shown in figure 10. In several cases, notably those in which the models were tested in the unmodified condition, the boundary layer appeared laminar on some wings and turbulent on others. On several of these tests with uncontrolled wing roughness, the rolling moments fell between the extremes set by the modified models.

The above discussion on aileron effectiveness at $M = 5.0$ also applies to that at $M = 2.2$, except that the effects of boundary-layer type are not adequately defined at the lower Mach number. The data that were recorded indicate a somewhat smaller effect of boundary-layer type at $M = 2.2$. It will be pointed out later that the difference in separated-region profile between laminar and turbulent flow at $M = 2.2$ is decidedly less pronounced than at $M = 5.0$, except at extremely small spoiler deflections. Hence it is not surprising that the rolling moments at $M = 2.2$ are not sensitive to this change of boundary-layer type.

At $h = 0.04c$, a model with polished wings exhibited the largest rolling moment for this spoiler height (see fig. 9(b)). Observation of the wing-tip-flow patterns for this test indicated that the boundary layer was turbulent on at least three wings. Therefore, this test is not in disagreement with the remainder of the data.

As will be discussed at length in a later section of this report, the increase in aileron effectiveness gained by fixing transition at the wing leading edge, particularly at $M = 5.0$, was not entirely explainable on the basis of simple two-dimensional-flow considerations alone. An additional difference between the two cases lies in the wing-tip leakage in the separated region. Figure 10 shows that the region in which wing-tip leakage of entrapped air occurs is much larger in the case of laminar flow. In order to see if this leakage influenced the effectiveness enough to explain the remainder of the laminar-turbulent difference several fixed-transition models were equipped with wing-tip fences. Pictorial evidence that this was effective in reducing leakage is given in figures 11(a) and 11(b). The rolling moments for these tests are given in figure 12 along with the previously shown data for similar models without fences. The fences increased the rolling effectiveness some 20 percent at $M = 5.0$. This suggests that the change in tip leakage was the primary difference between the laminar and turbulent boundary-layer cases. One model with polished wings was equipped with fences and tested successfully at $M = 2.2$. This test point is given in figure 12(b). In this case it was impossible to determine the presence or absence of boundary-layer transition since the wing-tip leakage was suppressed. The rolling moment exhibited by this model was essentially equal to that for similar models with saw-tooth leading edges.

The aileron effectiveness of trailing-edge spoilers has been treated above. An evaluation of spoilers as pitch controls, both as aerodynamic servos on all-movable wings and as direct controls, has been made in the appendix using the data of reference 4. The servo configuration promises to have great effectiveness with insignificant hinge moments. The direct control offers much lower effectiveness.

Two-Dimensional Flow and Profile Drag

Thus far the combined effects of Mach number and boundary-layer type on spoiler aileron effectiveness have been treated. Of comparable importance is the effect of these parameters on the drag of the spoilers in the absence of tip and fuselage effects. With the change in boundary layer, there occurs a striking change in flow pattern, a change which is quite clearly shown in the shadowgraphs of ring spoiler models in figure 13. For example, figures 13(a) and 13(b) compare the flow patterns with laminar and turbulent boundary layers, respectively, at $M = 5.0$ and $h/c = 0.04$. The separation point for the laminar-flow case is far forward

(here at the 0.45c point) while the separation for the turbulent-flow model occurs at the 0.85c point. The shock wave from the initial flow deflection is much weaker in the case of laminar flow than for turbulent flow. Downstream of the laminar separation point, eddies develop in the entrapped air and the separated boundary layer undergoes transition well ahead of the spoiler. Additional compression, much greater than the initial compression at laminar separation, occurs at transition and is evidenced by the strong shock waves emanating from this region. The pressure rise in the laminar-separation region is small compared to that in the turbulent region. Hence, when transition occurs between the laminar separation point and the spoiler, the main part of the induced normal force is associated with the turbulent portion. In figures 13(c) and 13(d), the same comparison is made for $M = 2.2$. Here, the same differences in flow occur as at $M = 5.0$, but the differences are not so pronounced.

Figures 13(e) and 13(f) show additional shadowgraphs of laminar- and turbulent-flow separation at $M = 5.0$, but at a smaller spoiler deflection than shown in figures 13(a) and 13(b). In figure 13(e) the boundary layer remained laminar over the top of the spoiler and beyond the base. Figure 13(g) shows that laminar flow can be maintained over a small spoiler at $M = 2.2$ also, but this was observed only at very low Reynolds numbers. Figures 13(e) and 13(g) are for the same spoiler deflection. Figure 13(h) shows one of the longer models and illustrates separation of a laminar boundary layer at $M = 2.2$. An additional shadowgraph of a ring spoiler model showing a broader view of the wake and trailing-shock-wave system is given in figure 13(i).

When the separation point moves back along the wing because of a change from laminar to turbulent boundary layer, two quantities which govern the incremental normal force are affected: the pressure in the separated region and the area over which it is applied. These two quantities are qualitatively compensating - as the pressure increases, the area decreases. Estimates of the over-all effect of the change in separation point on incremental normal force acting on the wings in two-dimensional flow were made. The loading corresponding to inviscid flow over a wedge extending from the separation point to the top of the spoiler was calculated from equations for oblique shock waves. This loading was then converted to rolling-moment coefficient for the present aileron models (wing-tip losses neglected) and is plotted in figure 14 as C_l versus the separation position for $h/c = 0.08$. The values of C_l in this figure are fortuitously close to the experimentally obtained values for $h/c = 0.08$. As the separation point moves back and the angle of flow separation increases, the calculated rolling moment increases because the incremental pressure increases faster than the affected area decreases. This is consistent with the observed relation between rolling moments with laminar and turbulent flow. Quantitatively, the calculated effect of moving the separation point from 0.10c to 0.70c is somewhat smaller than the experimental difference between laminar and turbulent cases at $M = 5.0$. Also, the assumption of a flat wedge filling the space between

the separation point and the spoiler is not strictly justifiable, particularly with laminar flow, since transition usually occurs ahead of the spoiler. The additional compression that occurs at transition makes the laminar-flow configuration more nearly equivalent to that with turbulent flow.

It was found that the incremental drag due to spoiler deflection could not be measured accurately with the aileron models because their decelerations were marginal, and appreciable corrections were required for drag due to lift. The ring models, therefore, were introduced primarily to make possible an accurate measurement of the drag penalty for spoiler deflection. The drag data obtained with these models are plotted in figure 15 against spoiler height, for laminar and turbulent flow at the two test Mach numbers. The drag associated with the larger spoilers is seen to be large compared to the drag of the clean configuration. At each Mach number, the Reynolds number is constant at the values shown. Cross plots were used to correct the data for small deviations from nominal Mach number. At both Mach numbers, two curves for laminar separation are presented. With small spoiler deflections, the flow remained laminar beyond the spoiler; in this case, the inside surface of the ring was kept smooth. With larger spoiler deflections, transition to turbulent-boundary-layer flow occurred ahead of the spoiler; here the internal boundary layer was tripped. This matching of internal flow was done in order to facilitate estimation of the pressure acting on the base. (See section on models.)

The drag coefficients in figure 15 are based on a constant reference area, namely the frontal area of the model with zero control deflection. It would be expected that the incremental drag of the spoiler would be primarily a function of the exposed frontal area of the spoiler and thus the data have been replotted in figure 16 as incremental drag coefficient, based on exposed spoiler frontal area, versus spoiler deflection. With turbulent boundary layer, figure 16(a), the incremental drag coefficient is constant at each Mach number, independent of spoiler height. To see if changing the Reynolds number would affect this result, tests were made with a threefold increase of Reynolds number. The results showed no effect of this change in Reynolds number. With laminar flow, figures 16(b) and 16(c), ΔC_D was no longer constant; it tended to increase with increasing spoiler deflection. Furthermore, there was an effect of Reynolds number.

Since both spoiler height and Reynolds number affected the incremental drag coefficient with laminar flow, it was suspected that their combined effects might be correlated on the basis of the ratio of spoiler height to boundary-layer thickness, which is proportional to $(h/c)\sqrt{R}$. The data are plotted in figures 16(b) and 16(c) in this form. The ratio $(h/c)\sqrt{R}$ was made to vary primarily by varying h. Additional points were obtained, however, by varying the air density (see fig. 13(g)) and by changing the model length (see fig. 13(h)). As seen in figure 16(b), M = 2.2, the

incremental drag coefficients for all conditions were reasonably correlated when plotted against $(h/c)\sqrt{R}$.

The variation in flow pattern with variation in $(h/c)\sqrt{R}$, as observed in shadowgraphs of ring models, was as follows. At small values of $(h/c)\sqrt{R}$, the transition point was downstream of the spoiler and the streamline slope just outside the separated region was small. With increasing values of $(h/c)\sqrt{R}$, the transition point moved forward ahead of the spoiler and the slope of the boundary between entrapped and moving air increased until, at a value of about 60, the transition point at $M = 2.2$ coincided with the separation point and the entrapped air space had the same appearance as that for turbulent-flow separation. Here the two incremental drag coefficients coincided.

The incremental drag coefficient for laminar flow at $M = 5.0$ is plotted in figure 16(c) against the variable $(h/c)\sqrt{R}$ and the relationship is similar to that at $M = 2.2$. However, at a spoiler deflection of about 0.07c ($(h/c)\sqrt{R} = 106$), the separation point for laminar flow would be near the end of the biconvex leading-edge section. For a spoiler height of 0.08c the boundary layer separated at this point; thus the angle of flow deflection was probably larger than it would have been had the model been longer. In recognition of this change in separation angle, the slope of the drag curve in figure 16(c) was made discontinuous at $(h/c)\sqrt{R} = 106$.

For comparison with the drag values in figure 16, there has been included the theoretical drag of a variable-chord 15° split flap with fully attached flow. With turbulent flow, the spoiler and flap drag are comparable though the spoiler does show higher drag. With laminar flow, at small deflections, the spoiler drag is smaller. While the spoiler drag is normally less with laminar than with turbulent flow, it will be recalled that the rolling effectiveness in the laminar case is also less than that with turbulent flow.

Because of its fundamental interest, the deduced average value of $\Delta P/q$ on the front face of the spoiler is also plotted (fig. 17). The base drag was estimated from references 8 and 9 and subtracted from the total drag-rise coefficient. The variation of skin friction caused by changes in wetted area on the ring models was estimated from data in reference 10. The skin-friction corrections were small and no appreciable error in $\Delta P/q$ would result from even a gross error in estimation. The base drag was about 40 percent as large as the pressure drag on the spoiler at $M = 2.2$ and about 15 percent as large at $M = 5.0$. If an error in base drag of 20 percent is assumed, the value of $\Delta P/q$ would be uncertain by 8 percent at $M = 2.2$ and by 3 percent at $M = 5.0$. The variation of $\Delta P/q$ looks very much the same as did the spoiler drag-rise coefficient but may be of greater interest because of its closer relationship to conditions in the separated region.

In running these tests, the increased stability of the laminar boundary layer with increased Mach number was very clearly shown. At $M = 2.2$, transition to turbulent flow occurred ahead of the spoiler for all values of $(h/c)\sqrt{R}$ above 12 while at $M = 5.0$, the transition point moved ahead of the spoiler only after a value of $(h/c)\sqrt{R}$ of 60 was reached. Also, in order to promote transition on the ring models tested at $M = 5.0$, the screw-thread trips had to be cut twice as deep as those on the $M = 2.2$ models and the Reynolds number per inch had to be increased by a factor of 2 by doubling the static pressure in the tunnel.

CONCLUSIONS

Free-flight measurements of rolling moments and drag have been made of trailing-edge spoilers on aspect-ratio-1 wings at Mach numbers of 2.2 and 5.0 and Reynolds numbers from 0.24 million to 3.50 million based on wing chord with both laminar and turbulent flow ahead of the separation point. The conclusions reached are given below.

1. Trailing-edge spoilers give rolling moments and drag comparable to that calculated for a 15° variable-chord split flap whose trailing edge is deflected to the height of the spoiler.

2. The change from laminar to turbulent flow affects the rolling moments. A 35-percent increase in rolling moment was observed for turbulent flow over that for laminar flow at $M = 5.0$.

3. Wing-tip fences, by eliminating tip leakage, produced a 20-percent increase in rolling-moment coefficient on models having turbulent boundary layers.

4. The spoiler drag-rise coefficient was independent of spoiler height and Reynolds number for both Mach numbers when transition was fixed ahead of the separation point. In the case of laminar flow ahead of separation, the drag coefficient was lower than that measured with turbulent flow for spoiler heights less than 0.08c.

Ames Aeronautical Laboratory
National Advisory Committee for Aeronautics
Moffett Field, Calif., June 15, 1955

APPENDIX

TWO SPOILER-CONTROL CONFIGURATIONS

The spoiler, in common with other wing-trailing-edge devices, has very limited capabilities at supersonic speeds. If the required control or maneuvering forces are greater than obtainable with these devices, one alternative is to use all-movable wings. These, in turn, require powerful actuators to overcome large hinge moments and are costly in terms of weight and complexity.

The possibility of using a spoiler as an aerodynamic servo to operate and stabilize an all-movable control deserves some attention. The following discussion is not an attempt to apply this concept to a real design, but, instead, is intended to illustrate the sort of performance which might be expected of such a system at Mach numbers below the hypersonic range. For contrast, an estimate of the effectiveness of a spoiler as a direct control on a missile is included.

Zero Hinge-Moment Servo

The control to be considered consists of an all-movable wing which is actuated and stabilized by means of a mechanically linked trailing-edge spoiler. In the interest of simplicity, the motion of only the wing and spoiler will be considered; the fuselage will be assumed to undergo no change in attitude. The external shape was chosen similar to the wing-spoiler combination of reference 4 (see fig. 18(a)) so that data from that reference could be used in this analysis. These data show that the spoiler can be used to actuate the wing without greatly affecting its lifting capabilities. The linkage is diagrammed in figure 18(b). The wing is mounted on its hinge axis, free to rotate, and its equilibrium position is controlled by the induced pressure field of the spoiler. To control the wing, only the spoiler is actuated. If the wing is disturbed from the desired setting of the control hub, δ_i, the spoiler is automatically moved so as to produce a load on the wing which tends to force the wing back to the desired setting. The sense of the gearing, then, is such that if the wing trailing edge is raised, by a gust, say, the spoiler will move up relative to it (see fig. 18(b)), and the resulting pressure field on the upper surface will tend to oppose the upward motion and minimize the error e. The error, e, which is the difference between the control hub setting δ_i and the angle of attack of the wing, will be zero at equilibrium for a balanced wing, that is, a wing with its center of pressure on the hinge line. For an unbalanced wing at equilibrium, the error e will be a function of the unbalancing moment that has to be overcome by the spoiler. At all times that this error e exists, the spoiler will be

deflected so as to reduce it. This tendency to stabilize the wing position about the desired position δ_i is used to control the position of the wing relative to the missile axis; δ_i is set and e is automatically minimized.

To see what response characteristics this type of system would have, a sample case is now developed. Both balanced and unbalanced wing combinations will be investigated at $M = 1.96$. In order to pick a hinge-line location for operation, the experimental center of pressure of this wing at $M = 1.41$ is used; this was approximately the 0.378-chord point for all values of δ up to 10°. Thus, the design Mach number can be considered to be 1.41 and the calculations are for the case of extreme overspeed flight. At $M = 1.96$, with the hinge line at 0.378c, the wing has restoring pitching moments below approximately 15° deflection as is shown in figure 19. The effect of assuming these moments to be zero will also be treated. In the off-design case, $M = 1.96$, wing pitching moments unbalanced, the spoiler must not only overcome the inertial moments, but must balance the aerodynamic moments of the wing as well. The gearing of the linkage system for this sample calculation was chosen such that a spoiler deflection of $h/c = 0.04$ resulted from an error of 1°. This gearing limits the trim error to about 1° at the chosen conditions. The pressure field of the spoiler was assumed to act at the 90-percent-chord point. This assumption, based on the 15° wedge analogy mentioned in the body of the report, was made to simplify the calculation of natural frequency of oscillation in e about the trim position δ. The undamped natural frequency may be expressed simply as

$$f = \frac{1}{2\pi}\sqrt{\frac{-(C_{m_e} + C_{m_\delta})qSc}{I_h}}$$

in which C_{m_e} is the stabilizing contribution of the spoiler and C_{m_δ} is the contribution, stable or unstable, of the wing alone. Clearly, $C_{m_e} + C_{m_\delta}$ is less than 0 if the system is statically stable. The importance of this natural frequency is that the response of the control improves as the natural frequency increases. The sample wing was a 6-percent-thick, half-solid, aluminum wing. The plan-form area was 1.5 square feet per panel. The flight conditions were Mach number of 1.96 and altitude of 40,000 feet. The natural frequency was calculated to be 36 cycles per second at $\delta = 0^\circ$, 39 cycles per second at $\delta = 4^\circ$, and about 27 cycles per second at $\delta = 15^\circ$. The approximate response curve for this unbalanced-wing case for an input signal calling for a change of δ from 0° to 5°, moving the control arm at 88° per second, is given in figure 20(a). As a comparison to the above result, the response curve for the balanced-wing case, C_{m_δ} assumed zero, is given in figure 20(b). Here a wing deflection of 5° was obtained about 14 percent faster than for the unbalanced configuration. In both of the above cases, aerodynamic damping was ignored.

The input rate for both cases was chosen such that the overshoot would not exceed 1°. This requirement could be relaxed in order to permit faster inputs. The spoiler deflection would occasionally exceed 0.08c in this case or, if stops were provided, would ride on the stops.

Direct Control

The capability of the same spoiler configuration used as a primary control instead of as a servo is also of interest. In this configuration the spoiler must cause rotation of the entire missile instead of the wings only, but the available moment arm is enough greater to offset some of this disadvantage. In order to investigate this point, calculations of the time to pitch a missile to 12° angle of attack were made. The missile chosen (see fig. 21) was 10 feet long and weighed 250 pounds and had fixed canard fins mounting trailing-edge spoilers. The flight conditions assumed were M = 1.96 at 40,000 feet altitude. The canard configuration was chosen because the spoilers are deflected toward the high-pressure side of the fins to produce trimming moments, which improves the spoiler effectiveness. A second advantage is that the lift produced directly by the spoilers is in the desired direction. The total fin plan area was 1.5 square feet with an aspect ratio of 2.7. The wing area is twice the fin area and the wings are so positioned as to give a static margin of 2 percent of the over-all missile length. The moment arm of the spoiler control is taken as 40 percent of the over-all length. Under these conditions the spoilers (deflected to h/c = 0.08) appear capable of trimming the missile to about 14° angle of attack. The time to pitch 12° is about 0.16 second allowing large overshoot. Since the lifting effectiveness of the entire missile is about twice that of the wings alone, the same maneuvering lift as that developed by the servo-control configuration could be attained here in about 0.11 second. On the other hand a glance at figure 21 shows that the fins and wings are large relative to the body; reducing the fin size would entail slower response characteristics.

REFERENCES

1. Patterson, R. T.: The Characteristics of Trailing-Edge Spoilers. Part I - The Effect of Turbulent-Boundary-Layer Thickness on the Characteristics of Two-Dimensional Spoilers at Two Supersonic Mach Numbers. AERO Rep. 827, pt. 1, David W. Taylor Model Basin, Aug. 1952.

2. Patterson, R. T.: The Characteristics of Trailing-Edge Spoilers. Part II - The Effects of Gap, Flap-Deflection Angle, Thickness, and Sweep Angle on the Aerodynamic Characteristics of Two-Dimensional Spoilers, and the Pressure Distribution Near the Tip of a Partial-Span Trailing-Edge Spoiler, at a Mach Number of 1.86. AERO Rep. 827, pt. 2, David W. Taylor Model Basin, Dec. 1952.

3. Patterson, R. T.: The Characteristics of Trailing-Edge Spoilers. Part III - The Normal-Force and Pitching-Moment Characteristics of Full- and Partial-Span Trailing-Edge Spoilers on Wedge Airfoils of Various Spans and Sweep Angles at Mach Numbers from 0.4 to 2.6. AERO Rep. 827, pt. 3, David W. Taylor Model Basin, Aug. 1953.

4. Jacobsen, Carl R.: Control Characteristics of Trailing-Edge Spoilers on Untapered Blunt Trailing-Edge Wings of Aspect Ratio 2.7 with 0° and 45° Sweepback at Mach Numbers of 1.41 and 1.96. NACA RM L52J28, 1952.

5. Czarnecki, K. R., and Lord, Douglas R.: Load Distributions Associated With Controls at Supersonic Speeds. NACA RM L53D15a, 1953.

6. Seiff, Alvin, James, Carlton S., Canning, Thomas N., and Boissevain, Alfred G.: The Ames Supersonic Free-Flight Wind Tunnel. NACA RM A52A24, 1952.

7. Harmon, Sidney M.: Stability Derivatives of Thin Rectangular Wings at Supersonic Speeds. Wing Diagonals Ahead of Tip Mach Lines. NACA TN 1706, 1948.

8. Love, Eugene S.: The Base Pressure at Supersonic Speeds on Two-Dimensional Airfoils and Bodies of Revolution (With and Without Fins) Having Turbulent Boundary Layers. NACA RM L53C02, 1953.

9. Chapman, Dean R., Wimbrow, William R., and Kester, Robert H.: Experimental Investigation of Base Pressure on Blunt-Trailing-Edge Wings at Supersonic Velocities. NACA Rep. 1109, 1952. (Supersedes NACA TN 2611)

10. Sommer, Simon C., and Short, Barbara J.: Free-Flight Measurements of Turbulent-Boundary-Layer Skin Friction in the Presence of Severe Aerodynamic Heating at Mach Numbers From 2.8 to 7.0. NACA TN 3391, 1955.

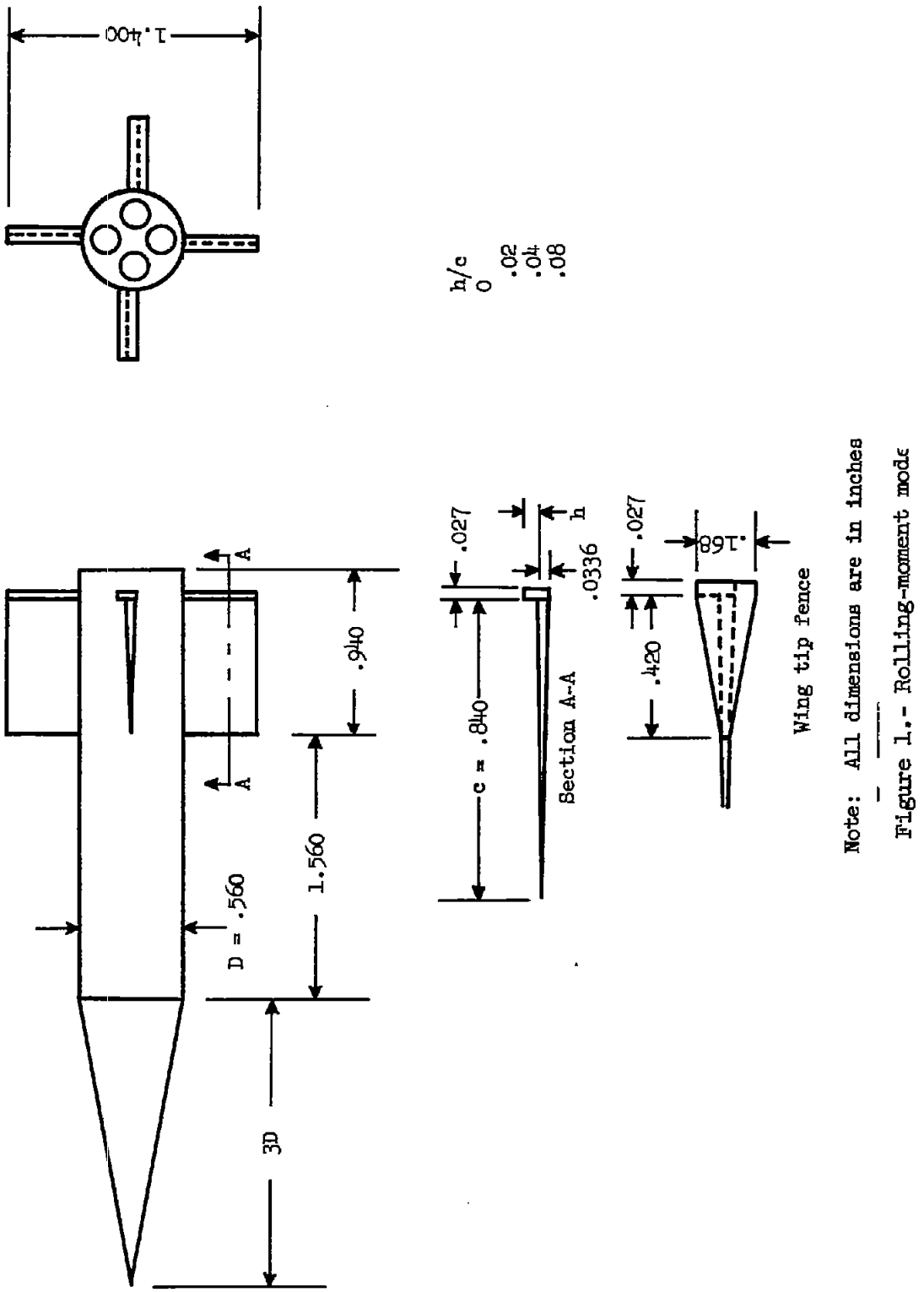

Note: All dimensions are in inches

Figure 1.- Rolling-moment mode

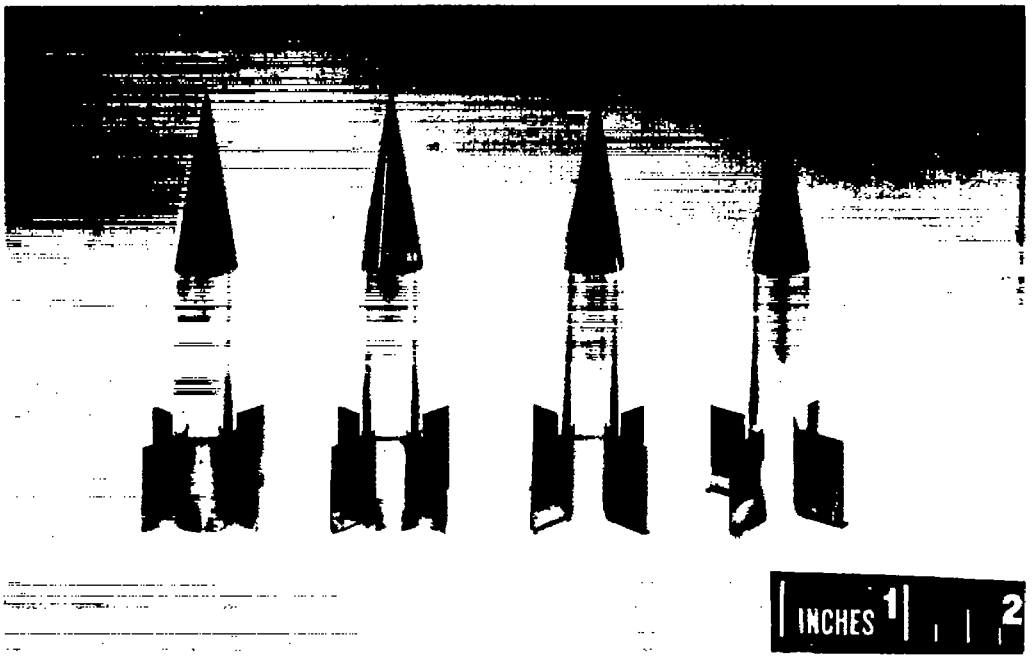

A-17546

(a) Aileron models with 0, 0.02c, 0.04c, and 0.08c spoiler deflections.

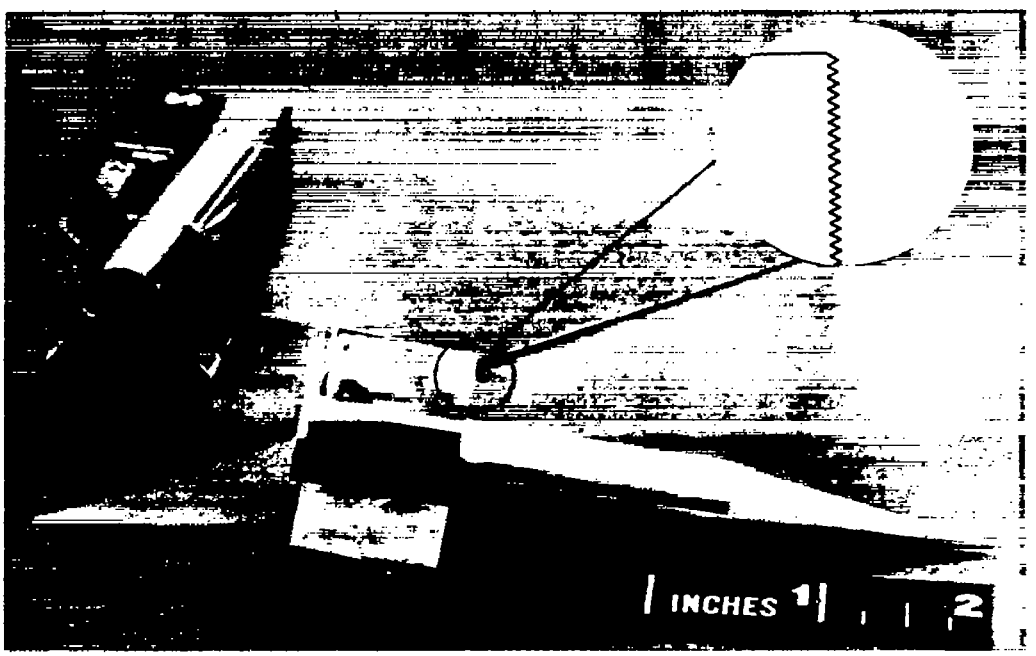

A-18240.1

(b) Modified aileron models with wing-tip fences and saw-tooth leading edges.

Figure 2.- Photographs of aileron effectiveness models.

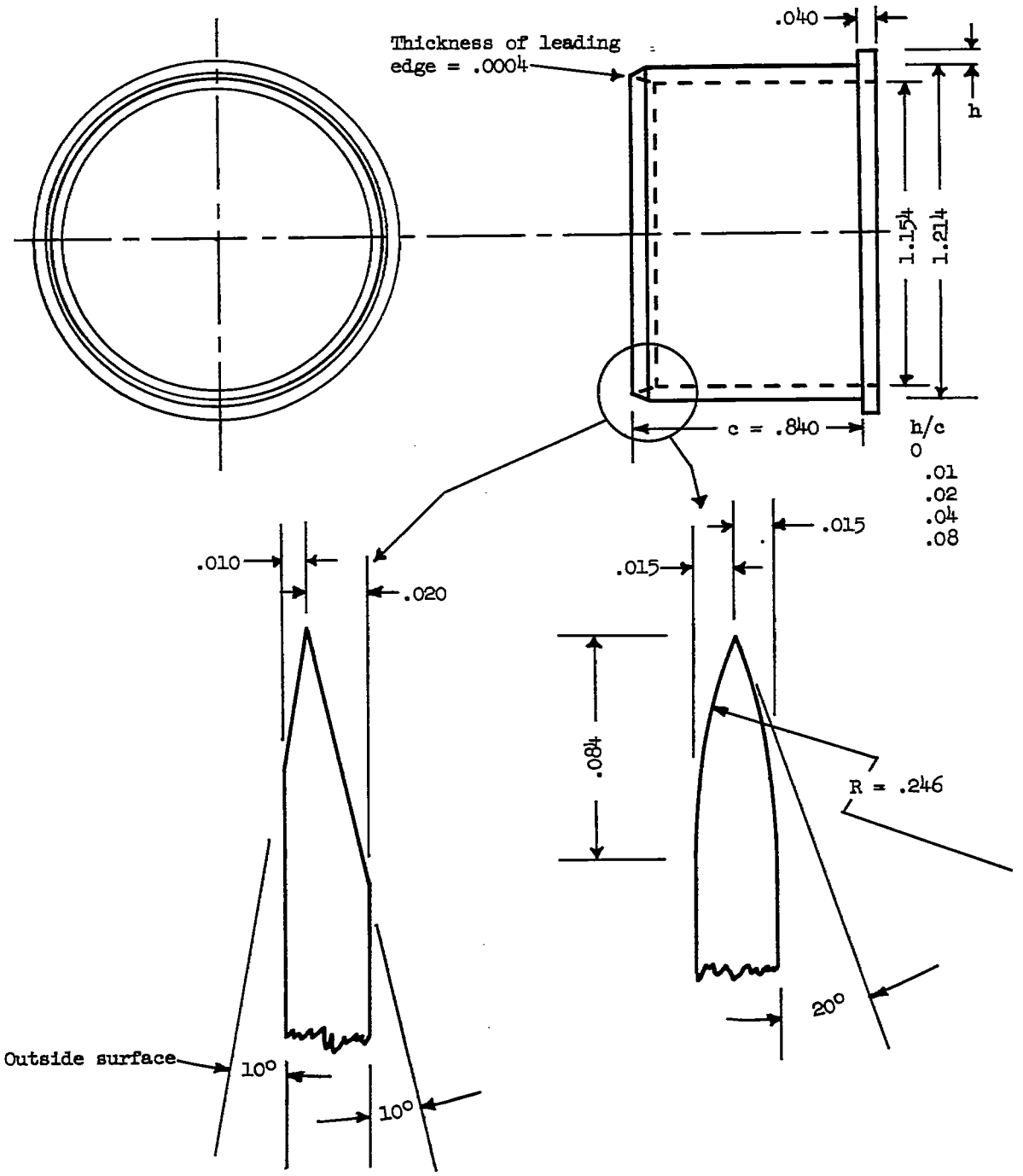

Note: All dimensions in inches

Figure 3.- Spoiler drag model.

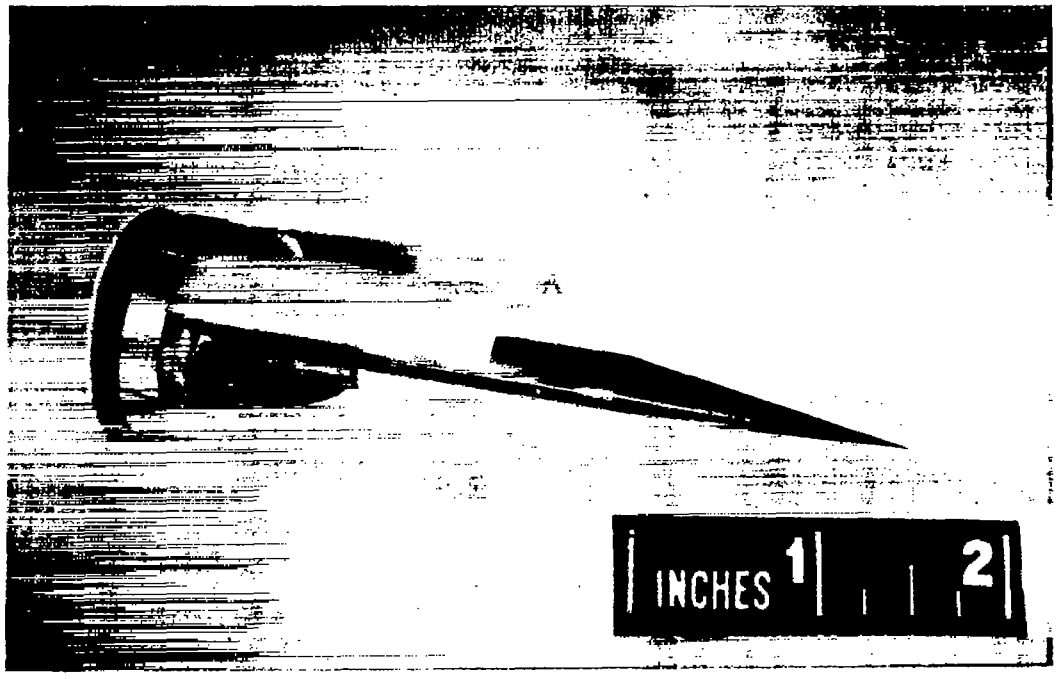

A-17547

Figure 4.- Aileron model in sabot assembly ready for launching.

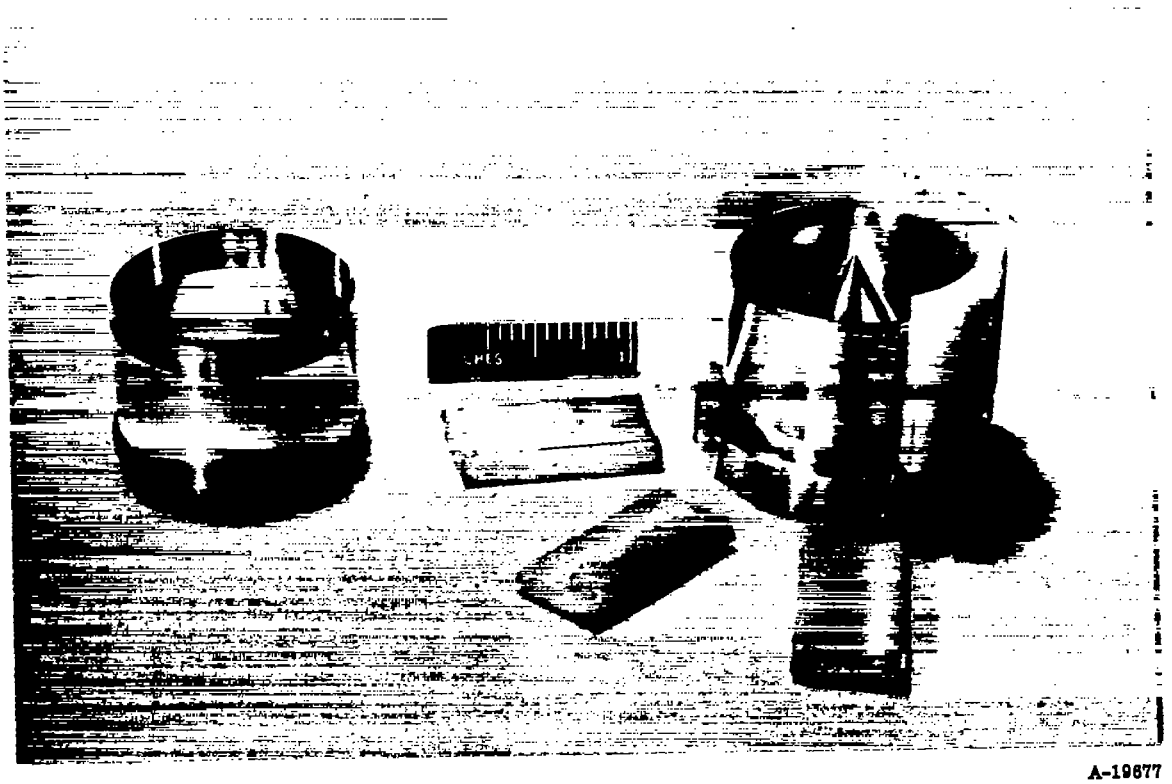

A-19677

Figure 5.- Photograph of ring spoiler model, and model and sabot assembly.

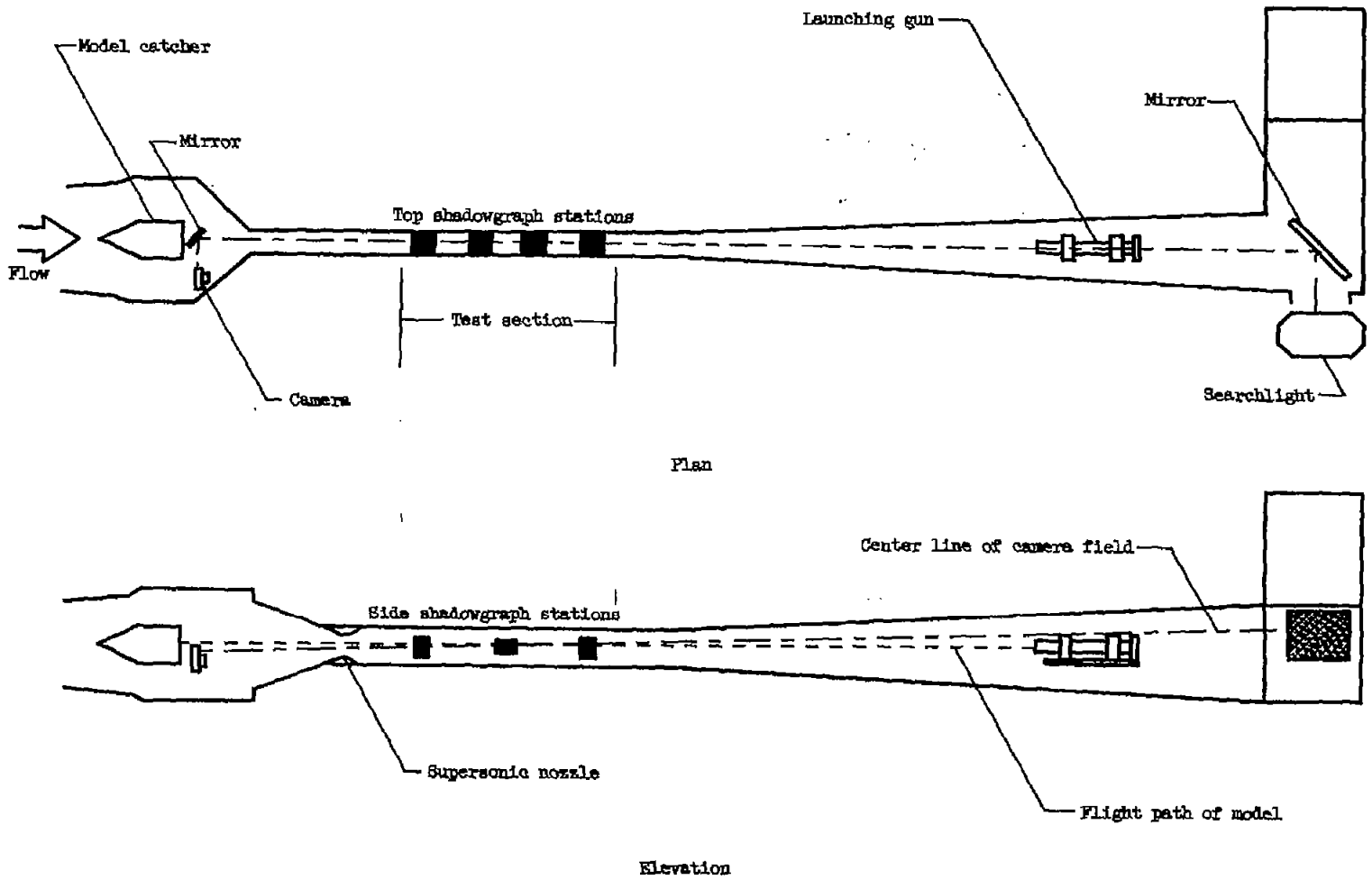

Figure 6.- Sketch of the Ames supersonic free-flight wind tunnel showing arrangement of equipment for photographing roll position.

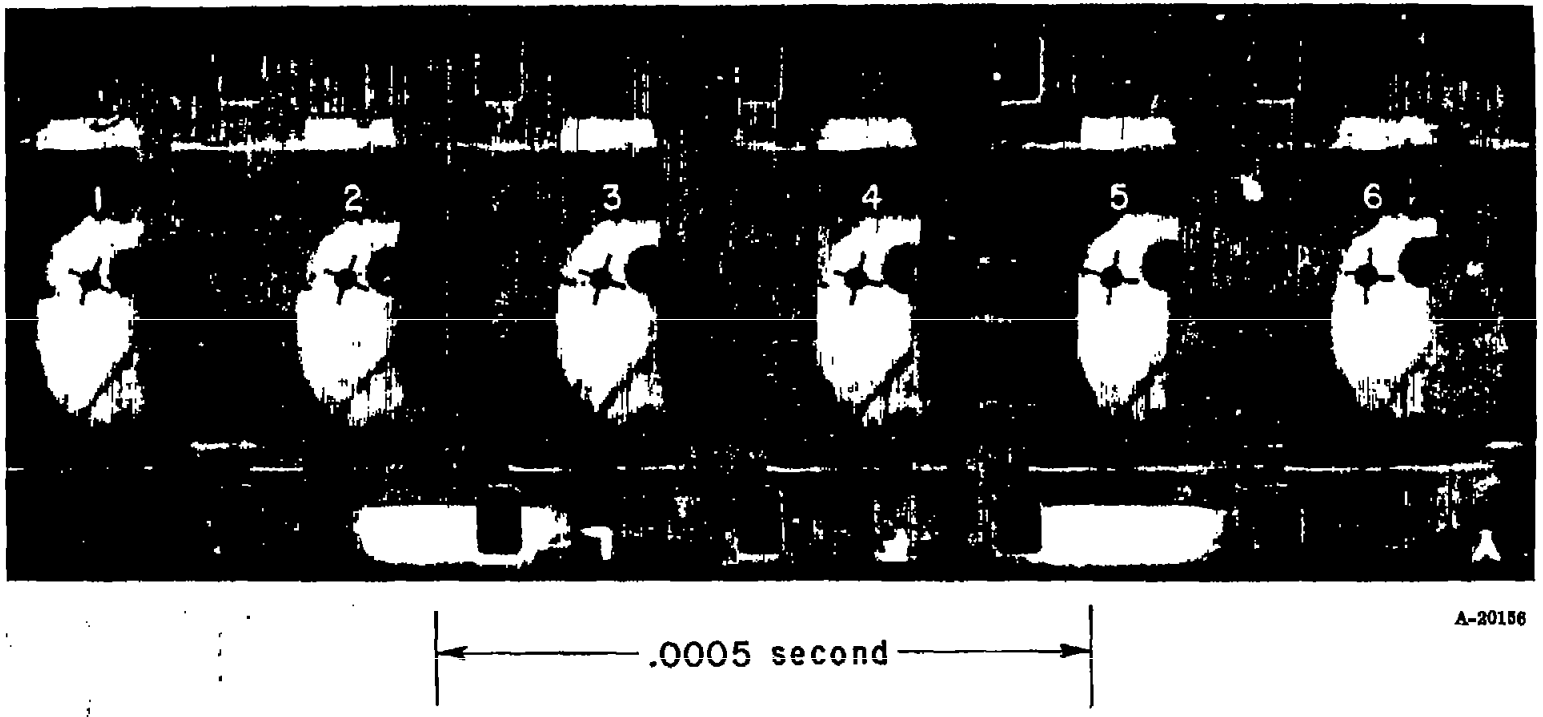

Figure 7.- Typical film record of spoiler effectiveness model.

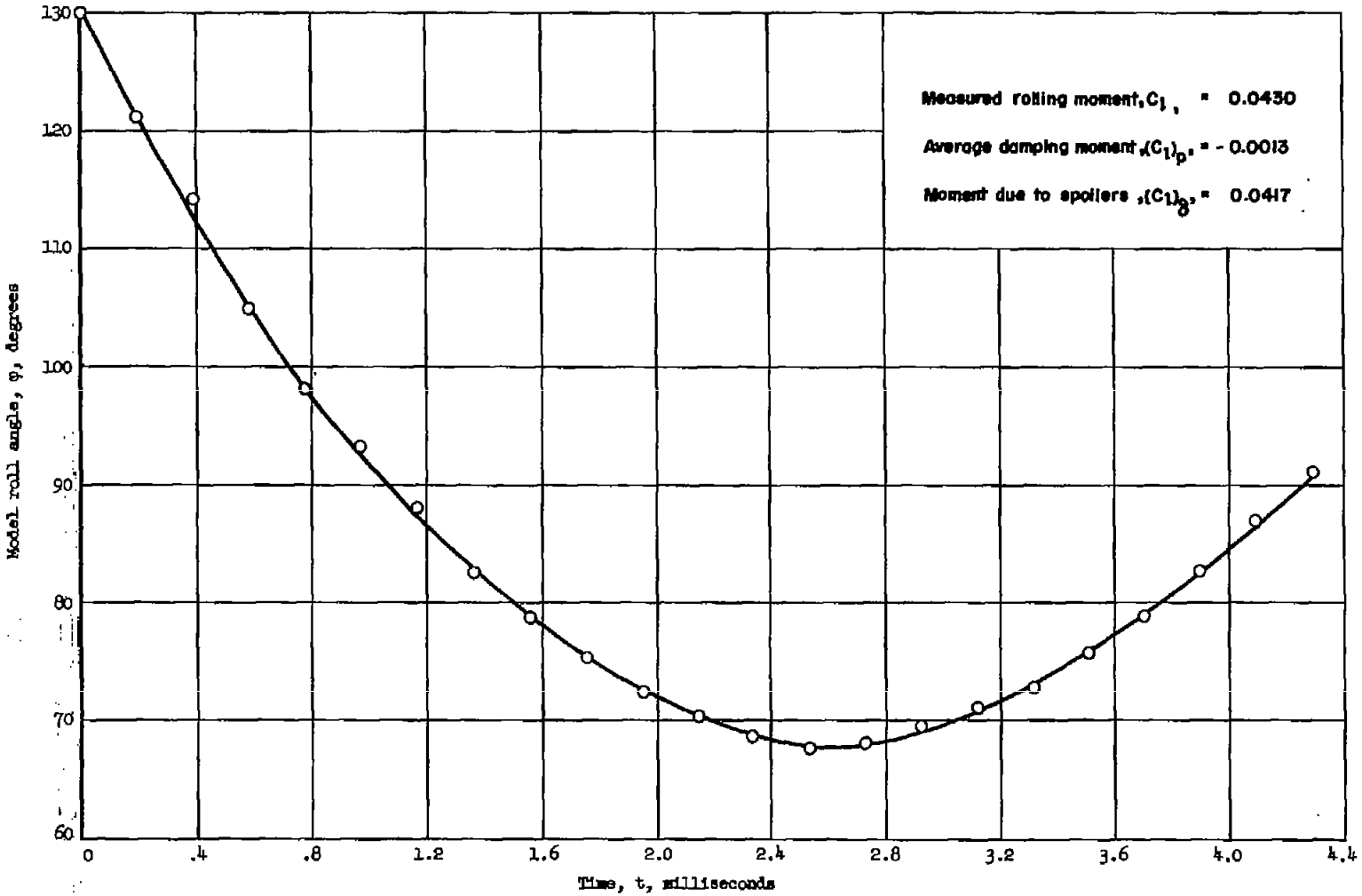

Figure 8.- Typical time history of model roll position.

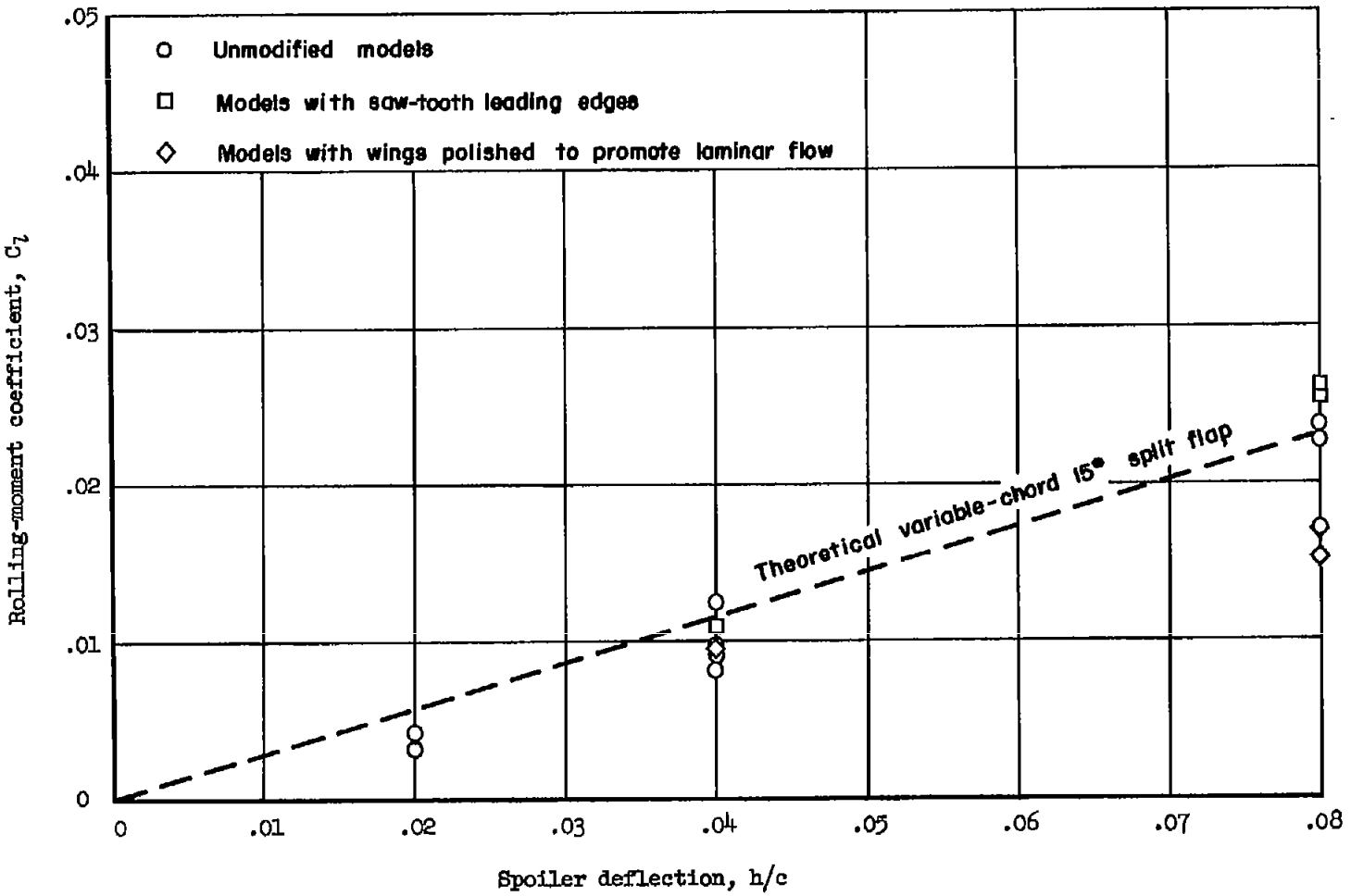

(a) M = 5.0, R = 1.5×10^6

Figure 9.- Variation of rolling-moment coefficient with spoiler deflection.

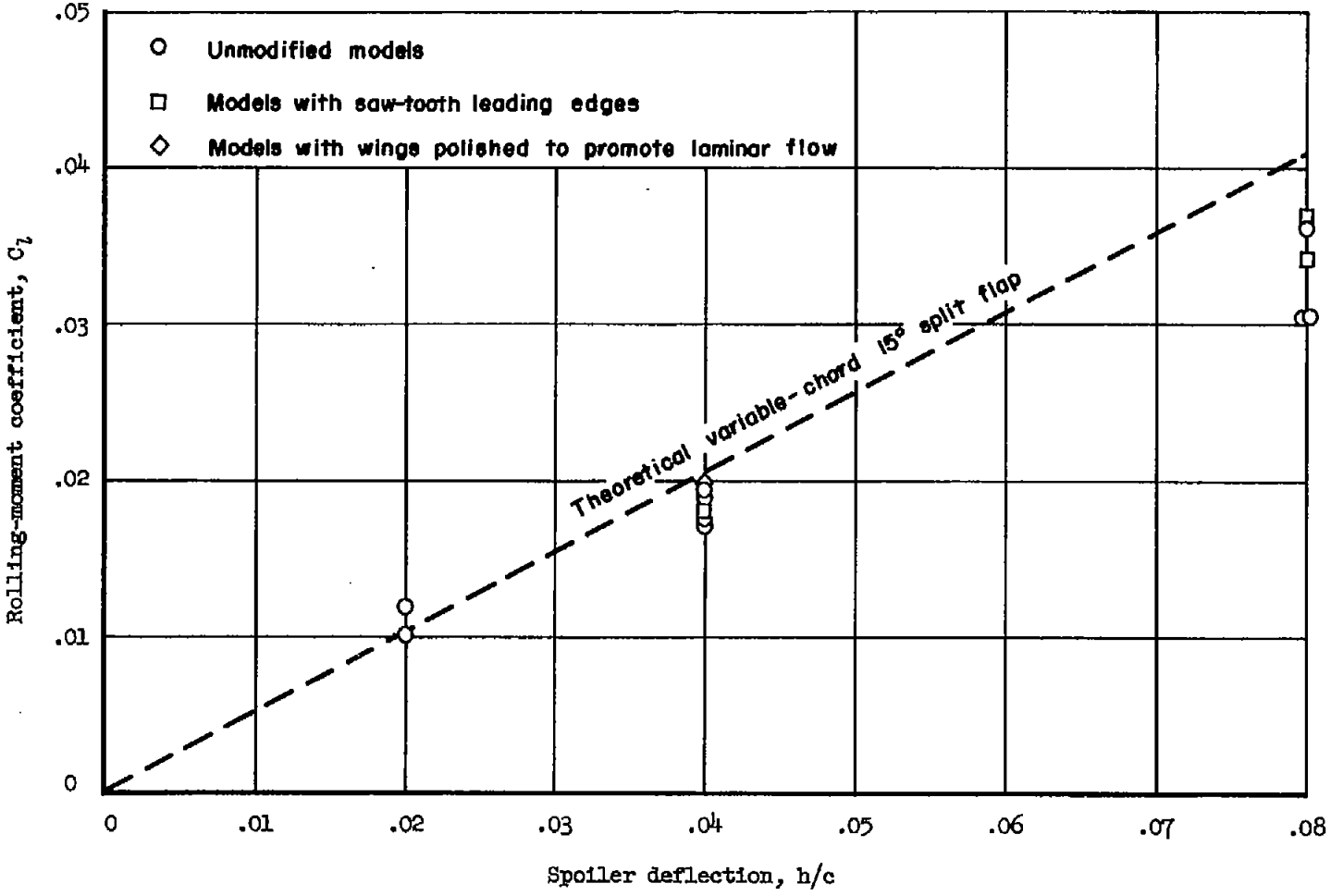

(b) M = 2.2, R = 1.15×10^6

Figure 9.- Concluded.

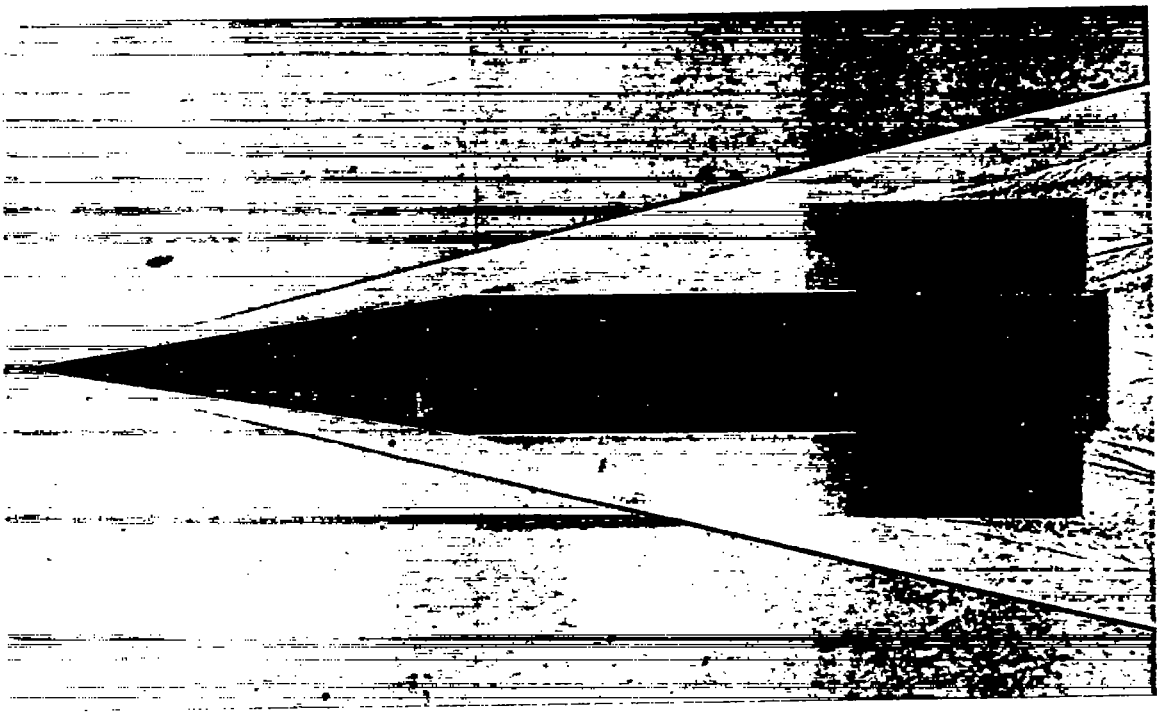

(a) Laminar separation, M = 5.0, R = 1.5×10^6, h/c = 0.08.

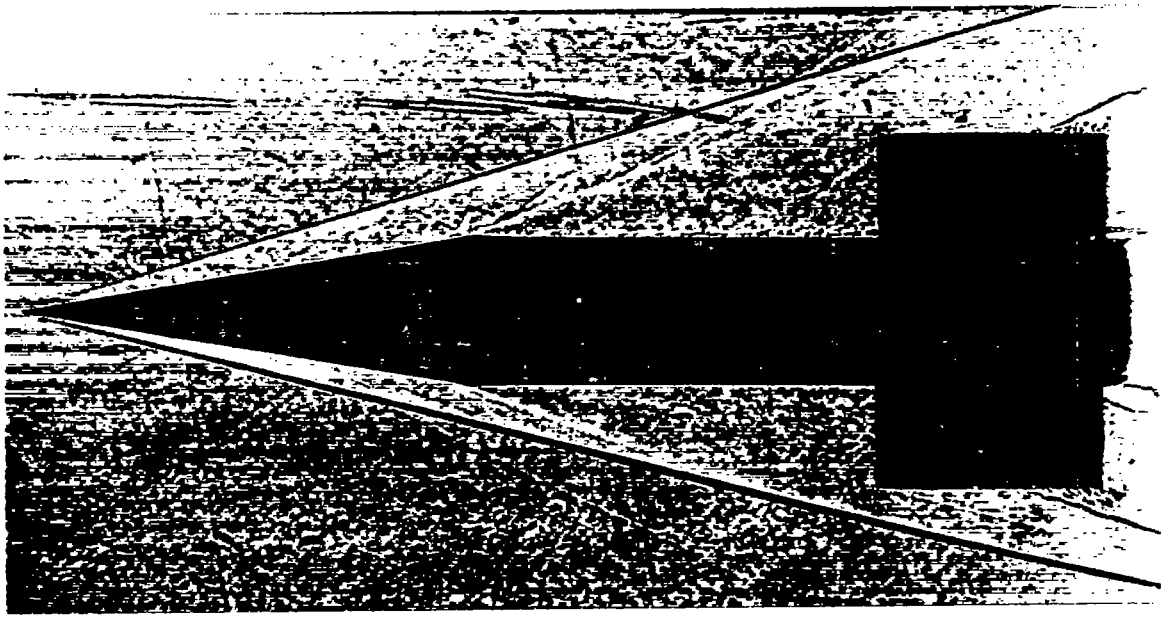

A-20157

(b) Turbulent separation, M = 5.0, R = 1.5×10^6, h/c = 0.08.

Figure 10.- Shadowgraphs of aileron models in flight.

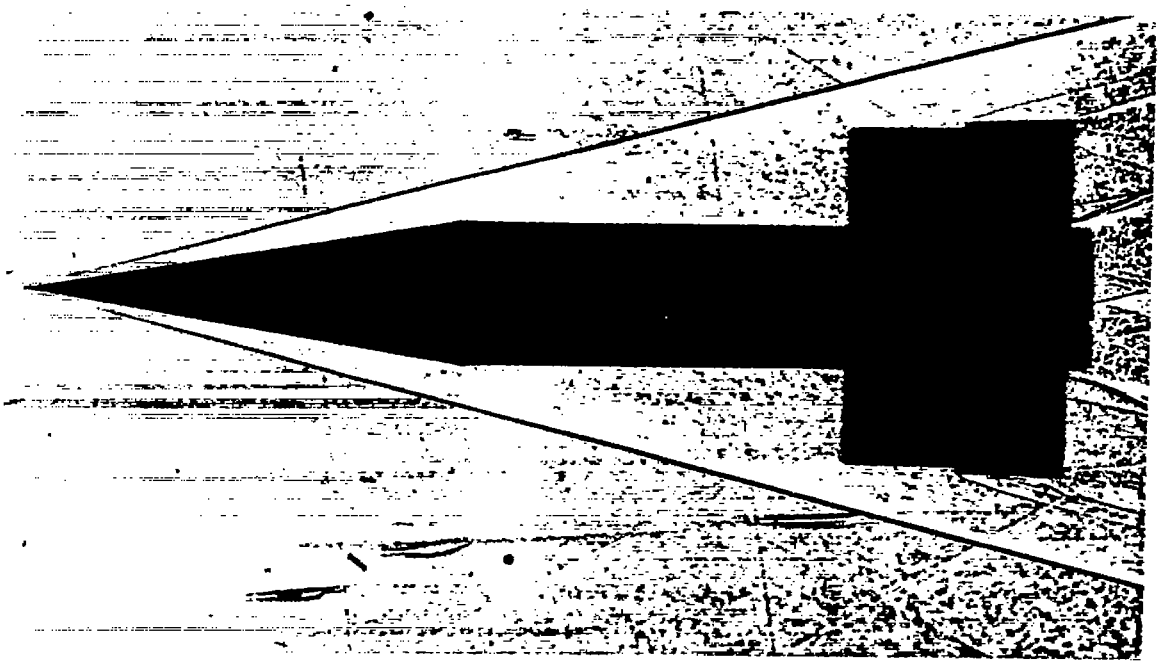

(a) Turbulent separation, with wing-tip fences; M = 5.0, R = 1.5×10^6, h/c = 0.08.

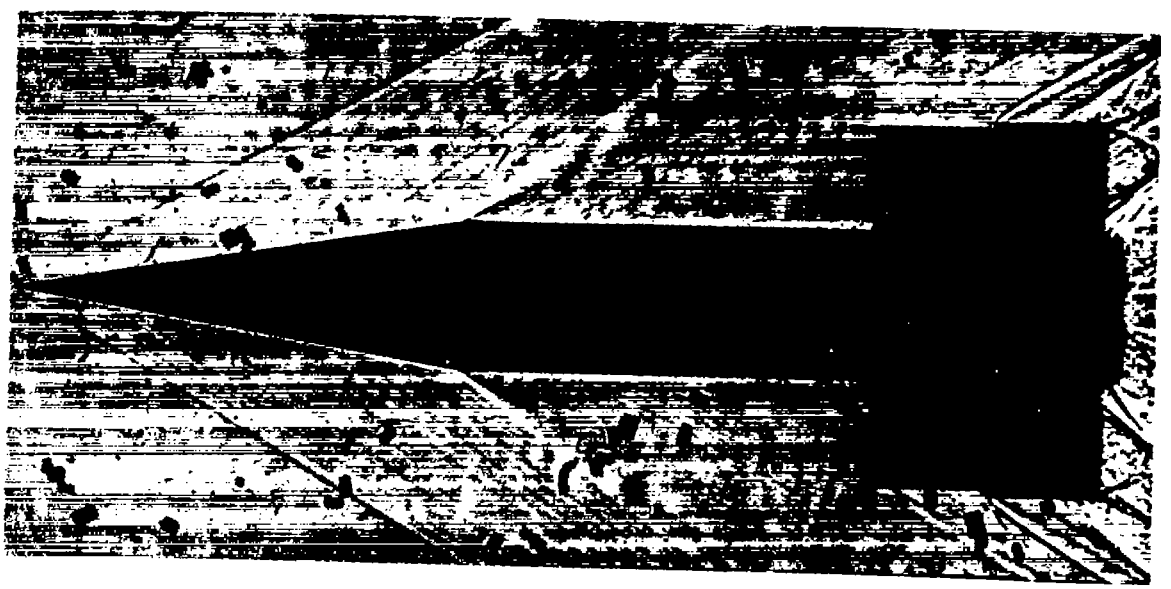

A-20158

(b) Turbulent separation, with wing-tip fences; M = 2.2, R = 1.15×10^6, h/c = 0.08

Figure 11.- Shadowgraphs of aileron models with wing-tip fences and turbulent separation.

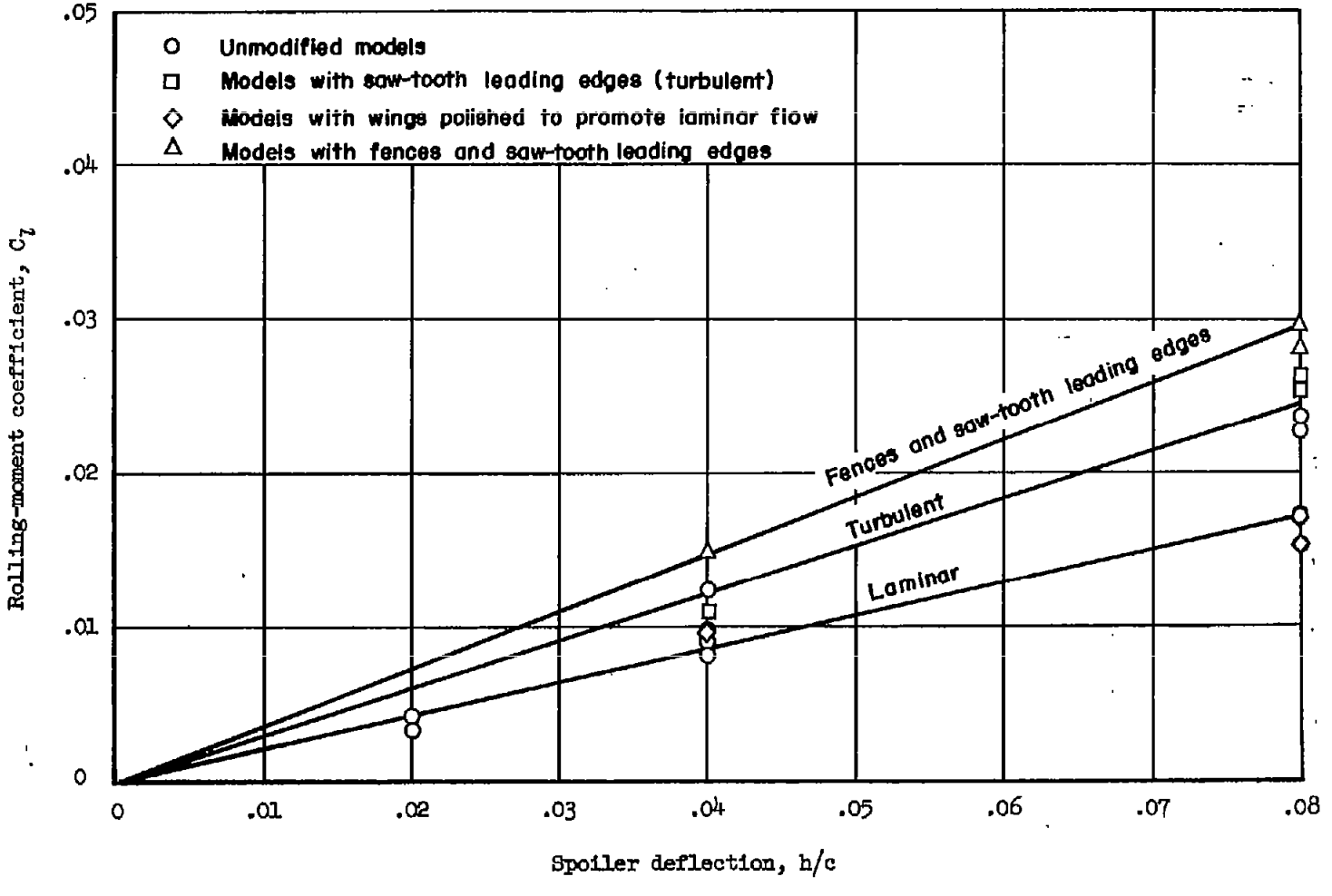

(a) M = 5.0, R = 1.5×10^6

Figure 12.- Effect of wing-tip fences on rolling-moment coefficient.

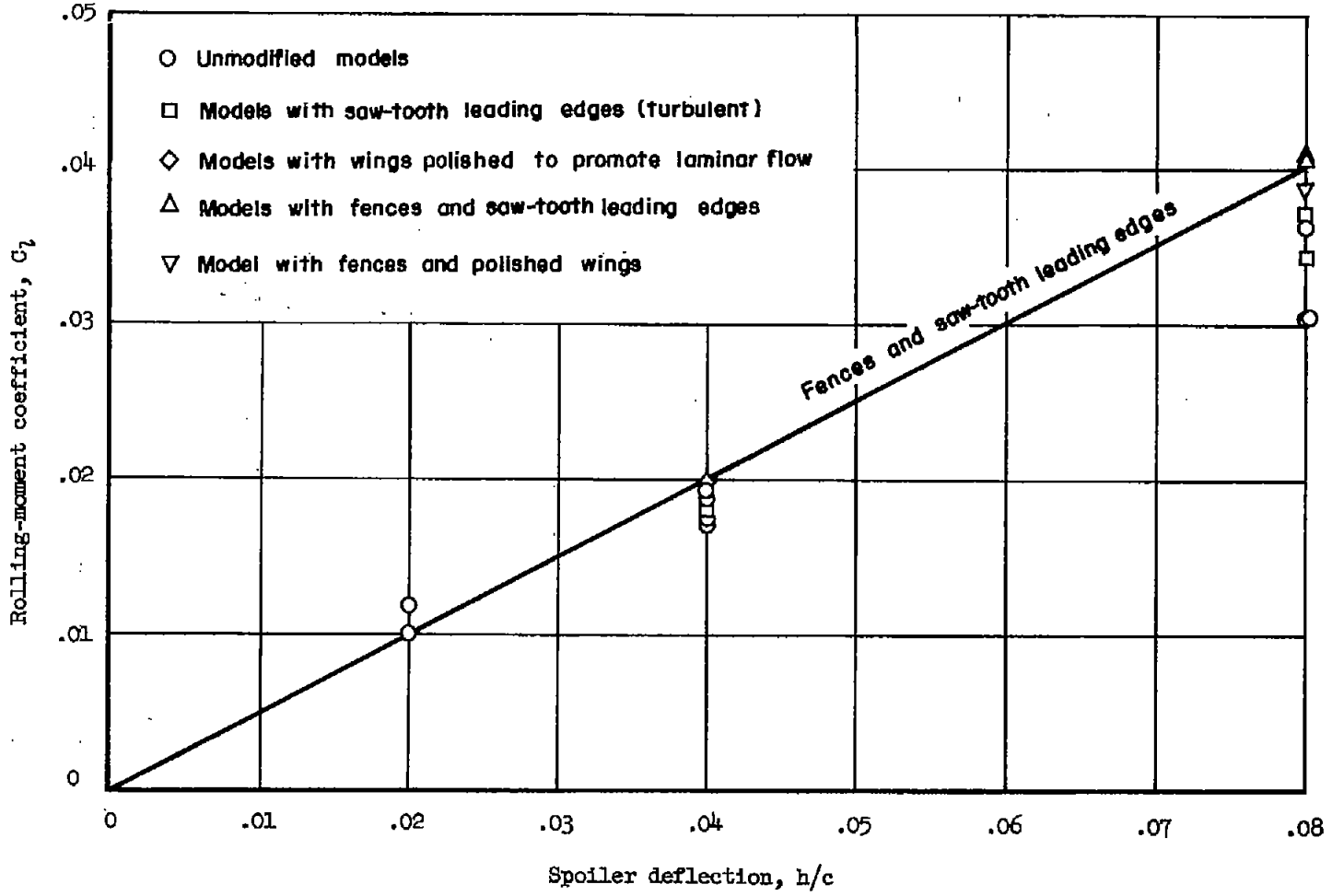

(b) M = 2.2, R = 1.15×10^6

Figure 12.- Concluded.

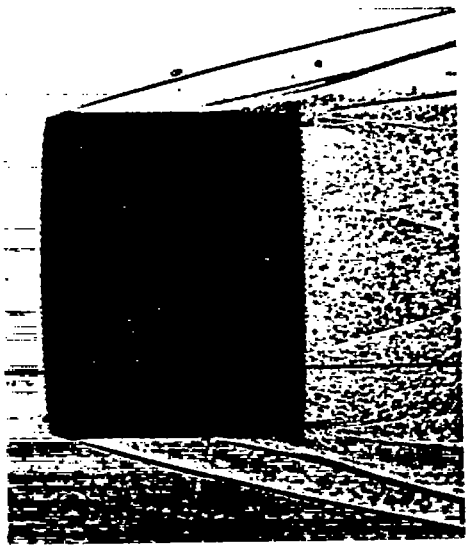

(a) Laminar ahead of separation; $M = 5.0$, $R = 2.2 \times 10^6$, $h/c = 0.04$.

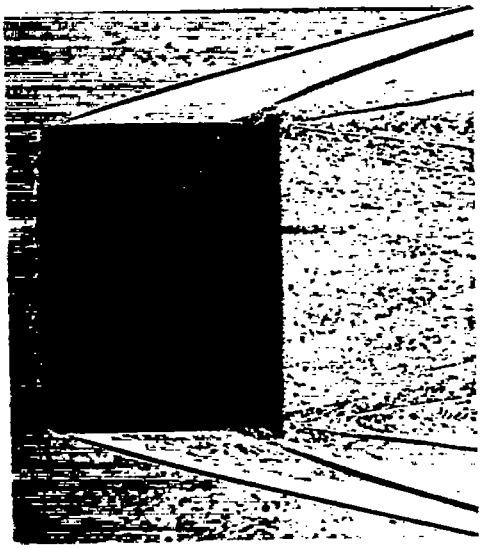

(b) Turbulent ahead of separation; $M = 5.0$, $R = 2.2 \times 10^6$, $h/c = 0.04$.

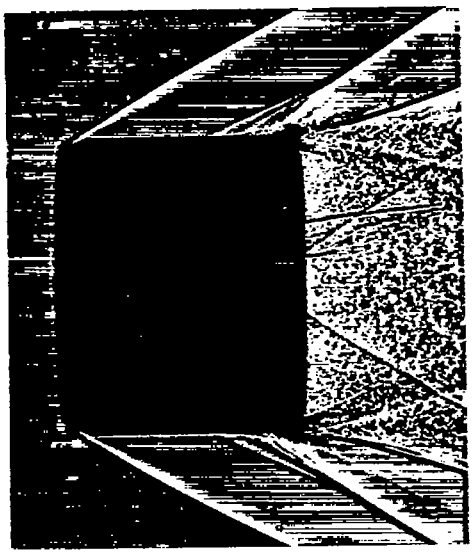

(c) Laminar ahead of separation; $M = 2.2$, $R = 1.15 \times 10^6$, $h/c = 0.04$.

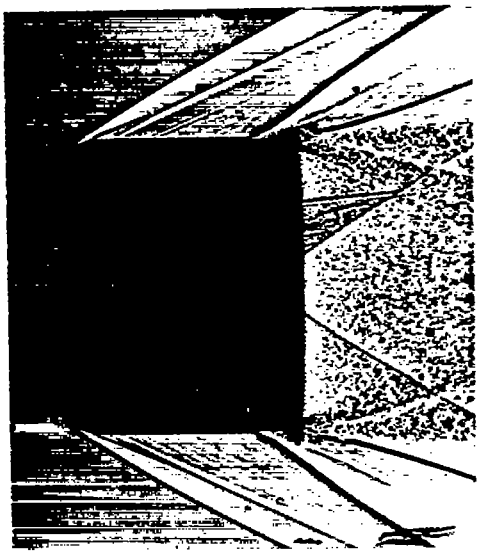

A-20159

(d) Turbulent ahead of separation; $M = 2.2$, $R = 1.15 \times 10^6$, $h/c = 0.04$.

Figure 13.- Shadowgraphs of ring spoiler models.

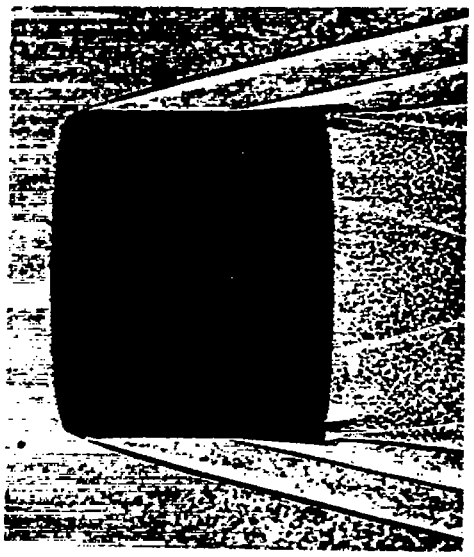

(e) Laminar ahead of separation; M = 5.0, R = 2.2×10^6, h/c = 0.02.

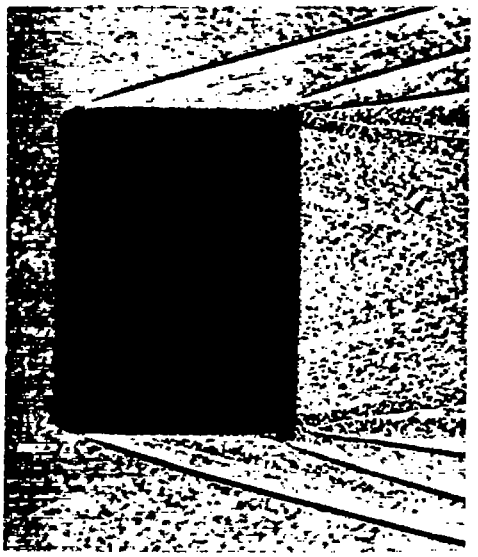

(f) Turbulent ahead of separation; M = 5.0, R = 2.2×10^6, h/c = 0.02.

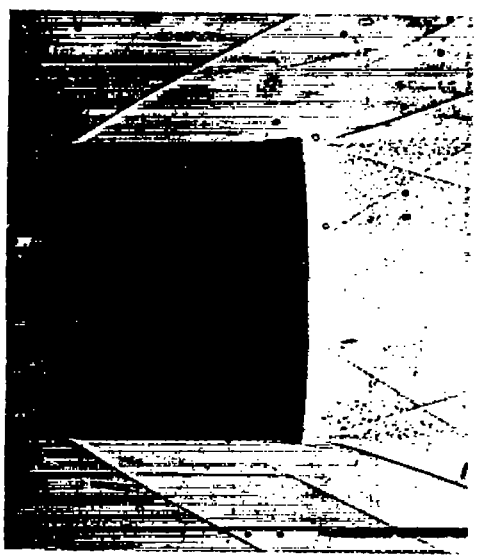

(g) Laminar ahead of separation; M = 2.2, R = 0.24×10^6, h/c = 0.02.

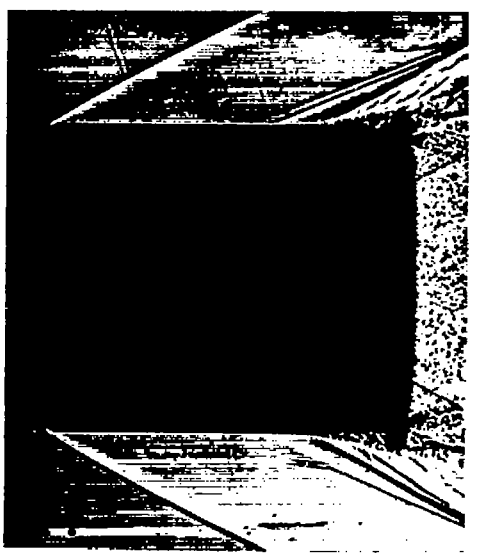

A-20160

(h) Laminar ahead of separation; M = 2.2, R = 1.87×10^6, h/c = 0.04.

Figure 13.- Continued.

[redacted]

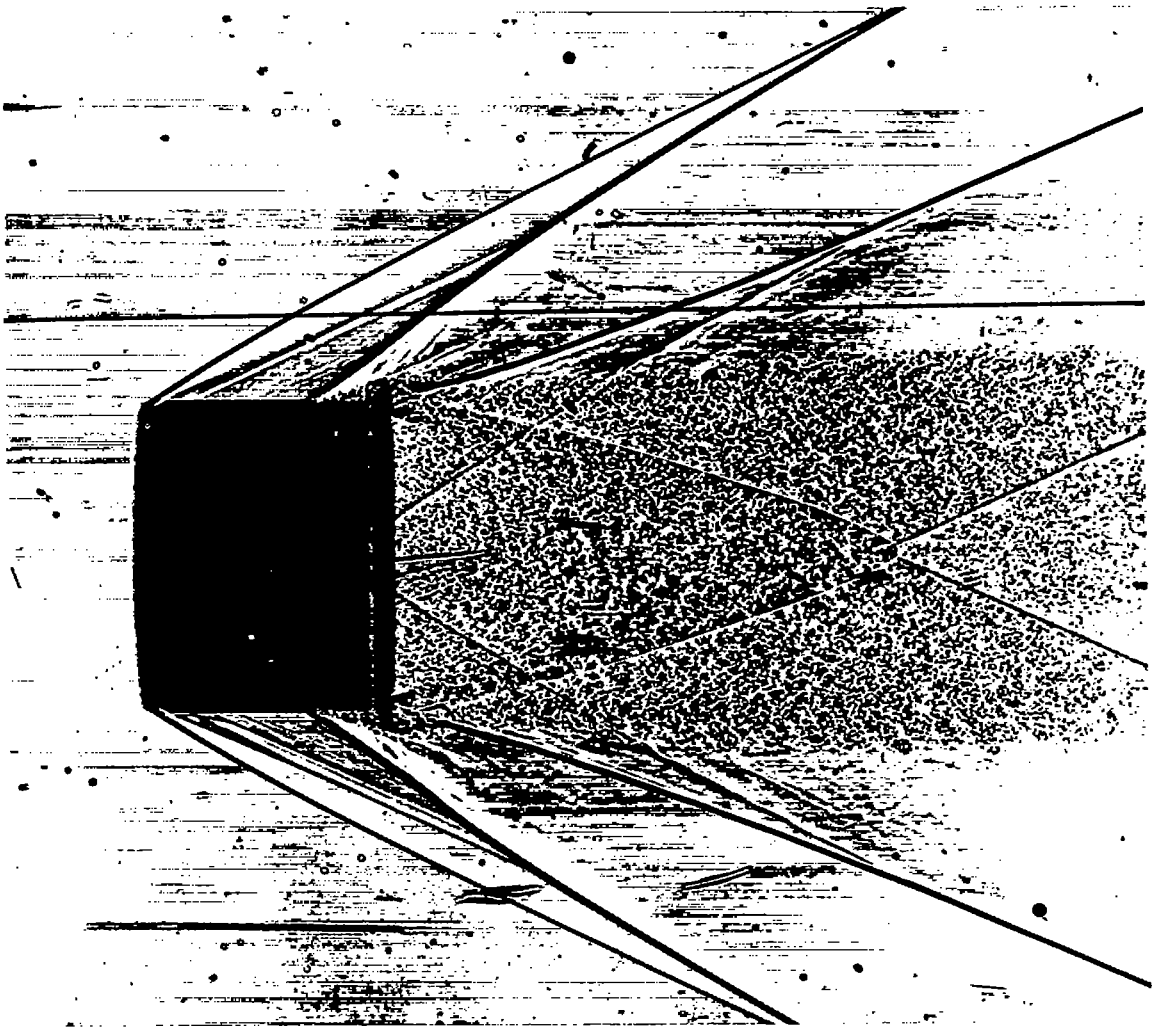

A-20161

(i) Turbulent ahead of separation; M = 2.2, R = 1.15×10^6, h/c = 0.08.

Figure 13.- Concluded.

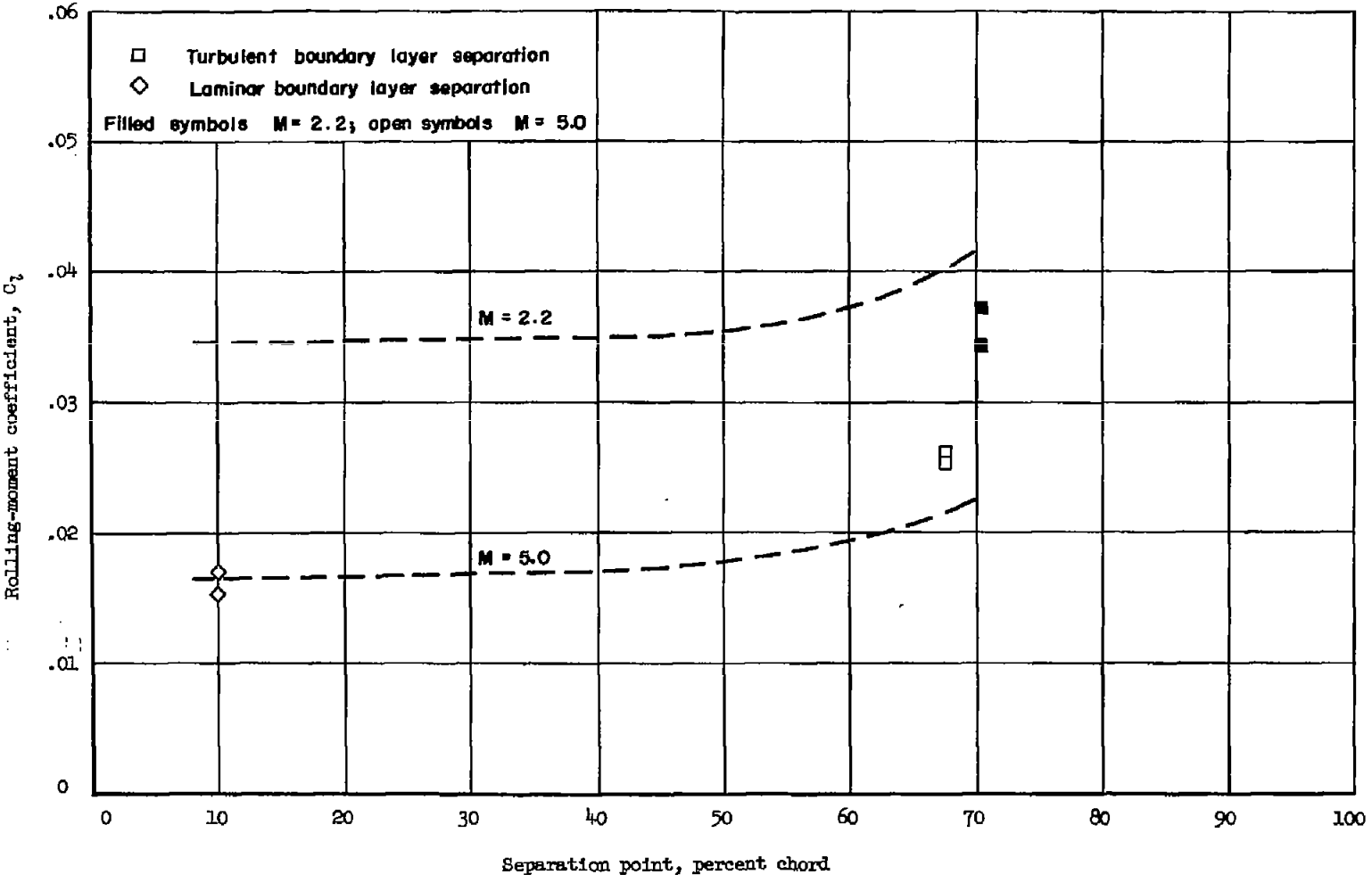

Figure 14.- Experimental and theoretical variation of rolling-moment coefficient with separation position; h/c = 0.08.

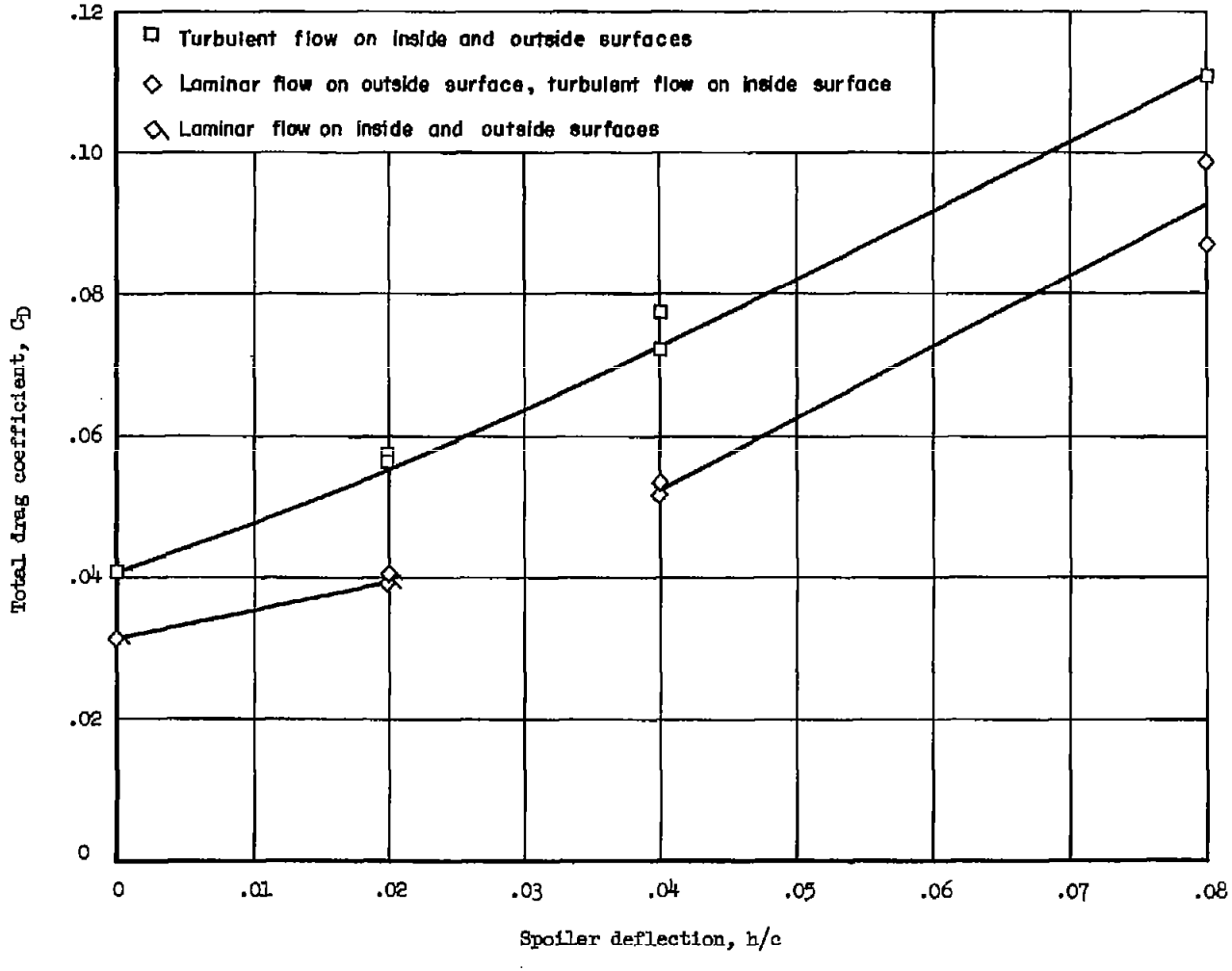

(a) M = 5.0, R = 2.2×10^6

Figure 15.- Total drag-coefficient variation with spoiler deflection.

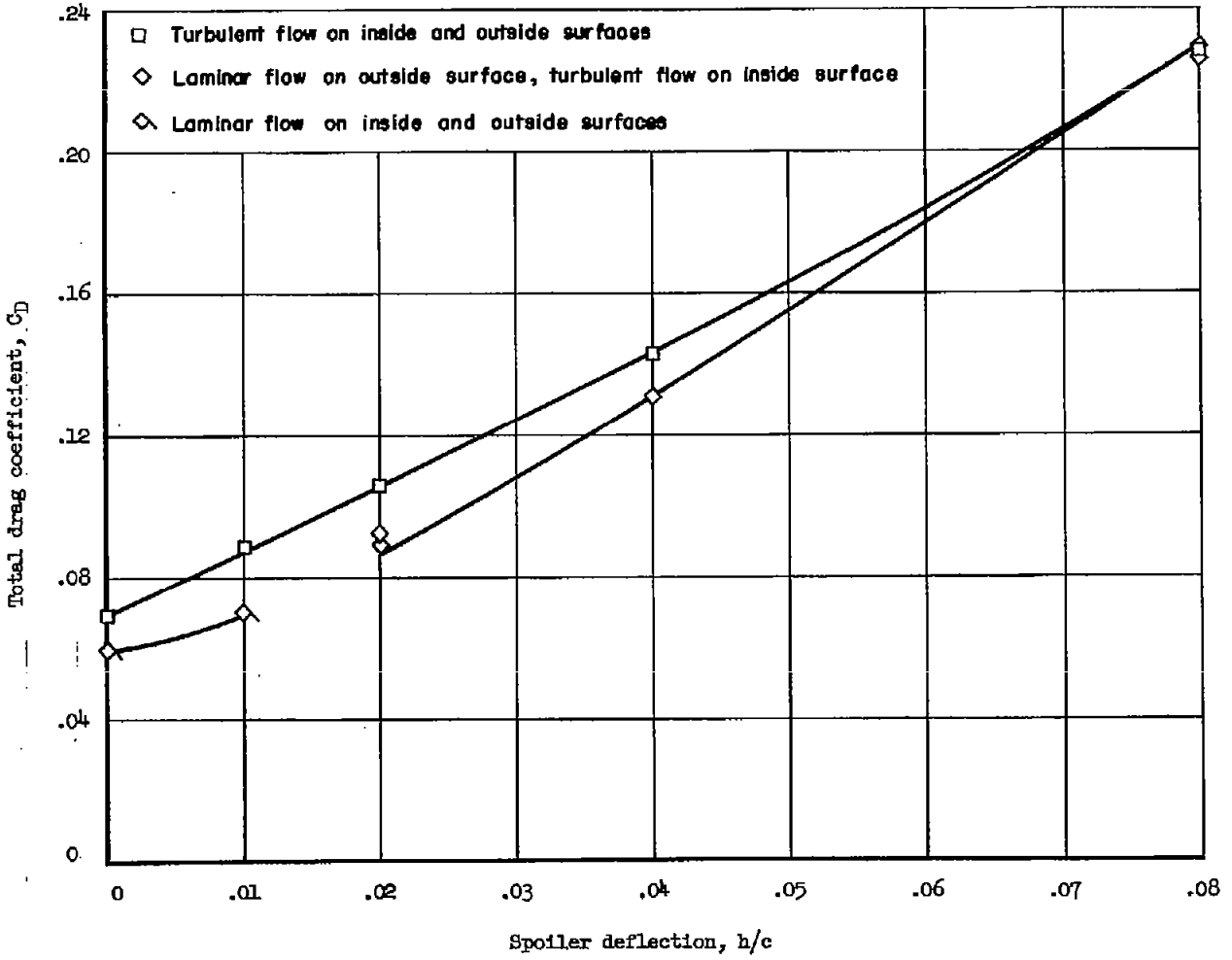

(b) M = 2.2, R = 1.15×10^6

Figure 15.- Concluded.

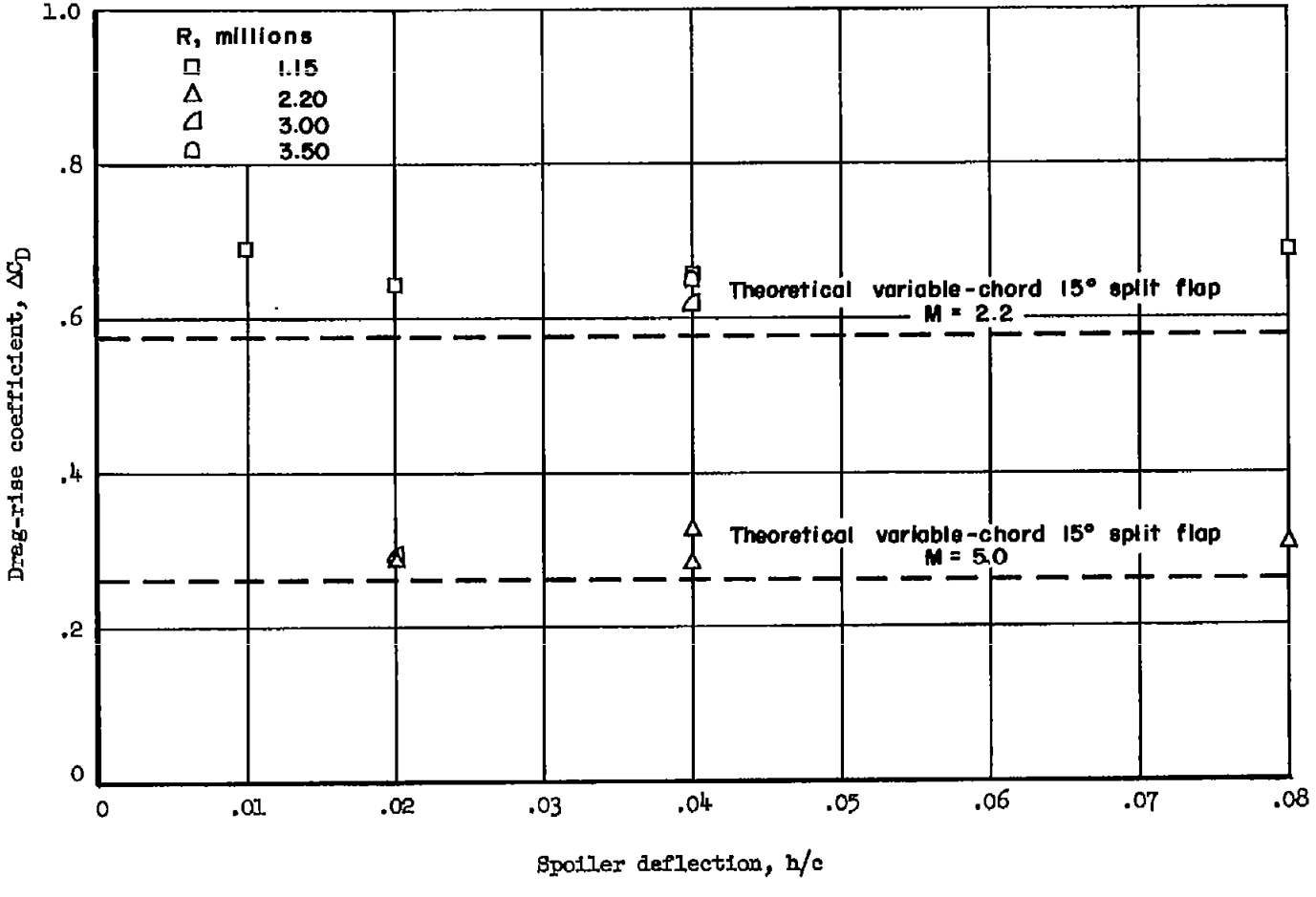

(a) Turbulent boundary-layer separation; M = 2.2 and M = 5.0.

Figure 16.- Variation of drag-rise coefficient with spoiler deflection.

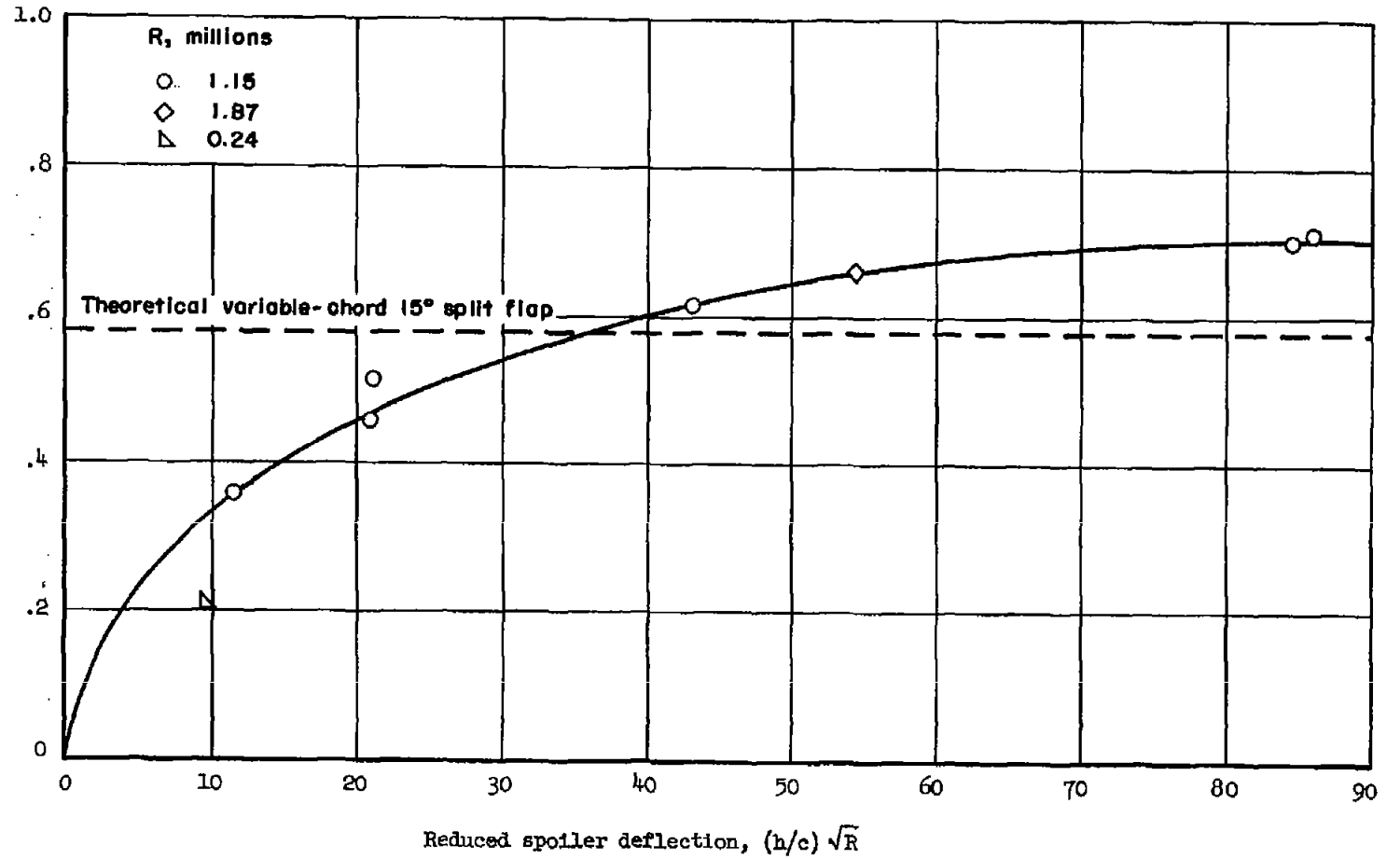

(b) Laminar boundary-layer separation; M = 2.2.

Figure 16.- Continued.

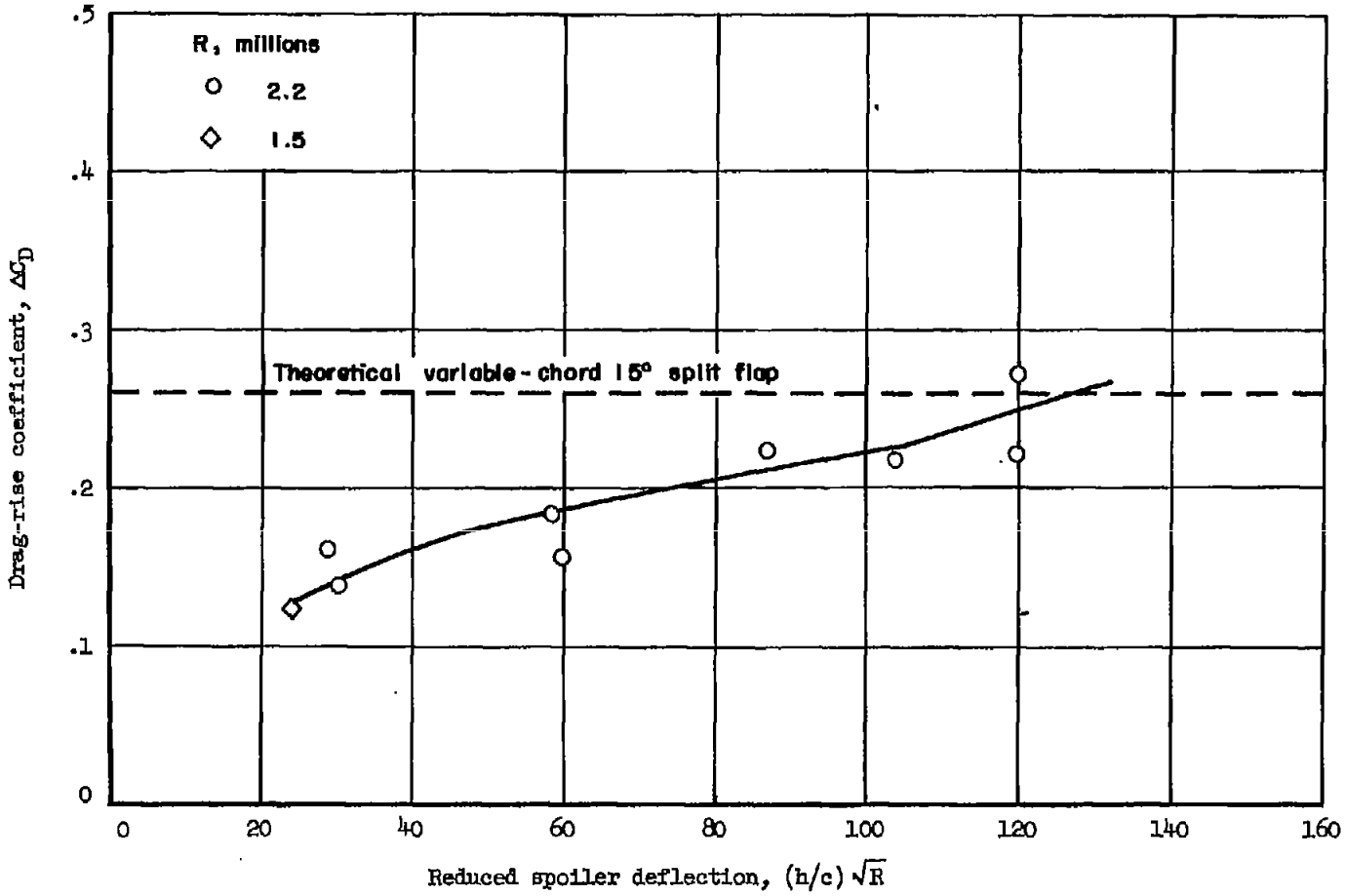

(c) Laminar boundary-layer separation; M = 5.0.

Figure 16.- Concluded.

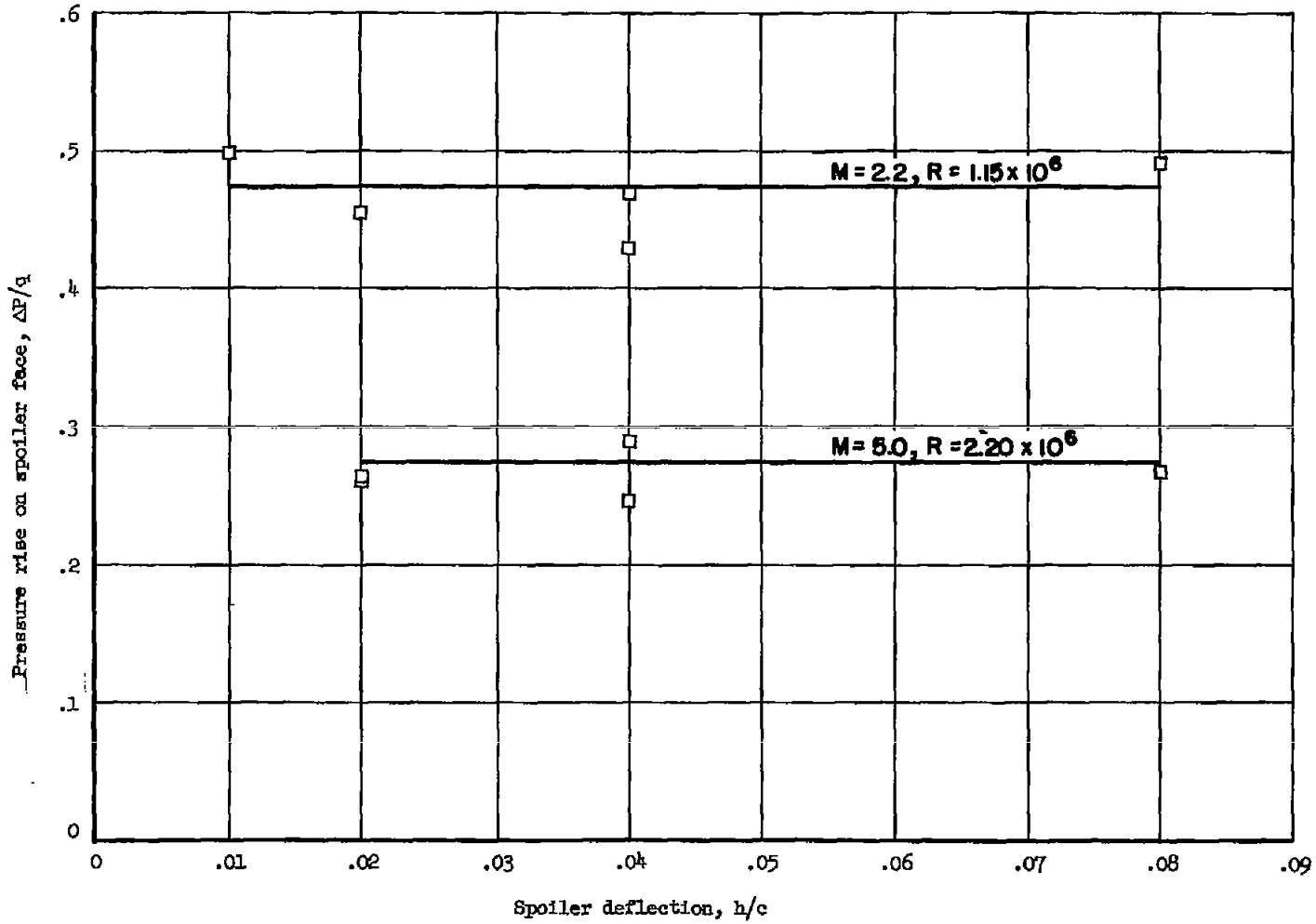

(a) Turbulent separation; M = 2.2 and 5.0.

Figure 17.- Variation of mean pressure rise on spoiler face with spoiler deflection.

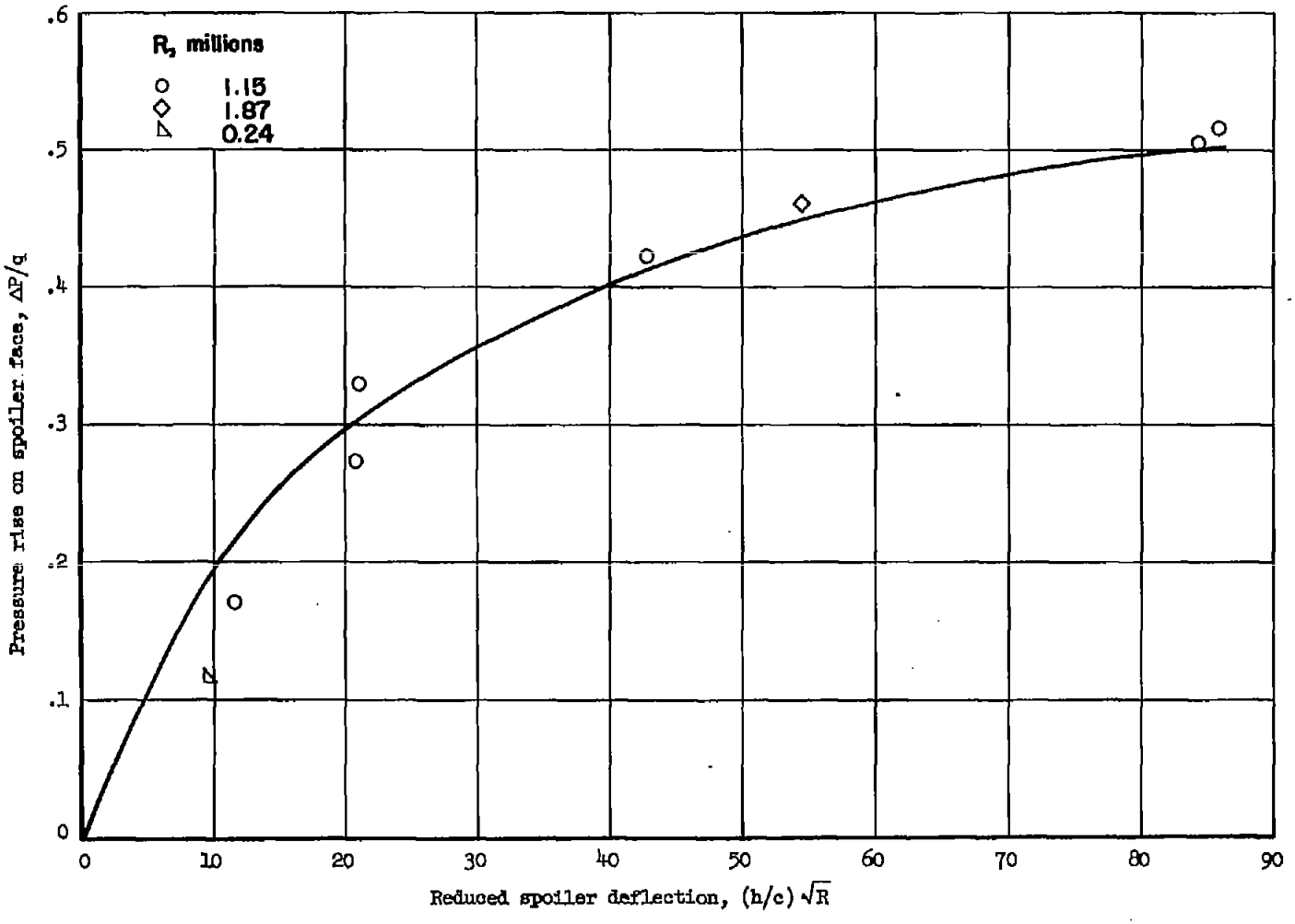

(b) Laminar separation; M = 2.2.

Figure 17.- Continued.

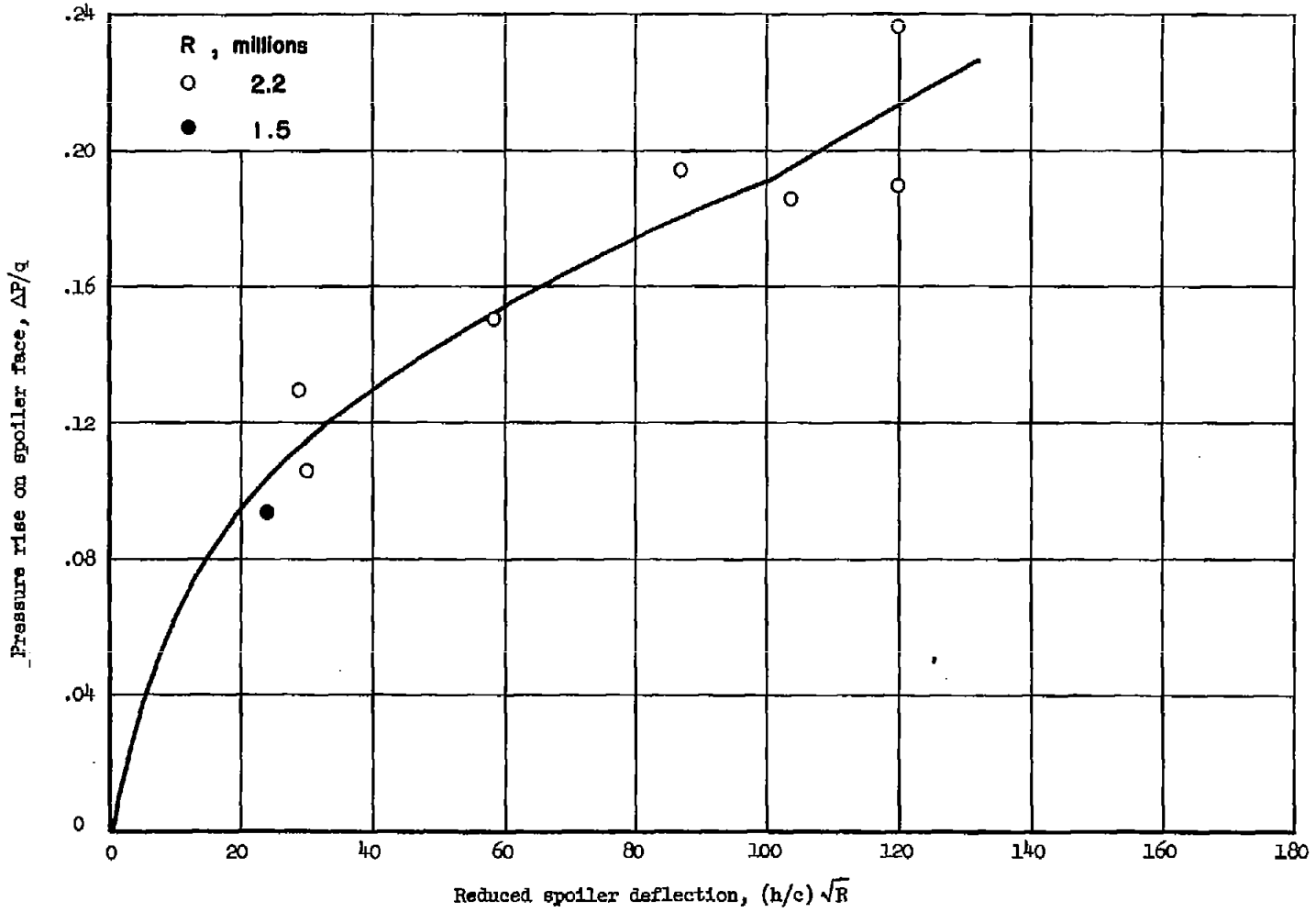

(c) Laminar separation; M = 5.0.

Figure 17.- Concluded.

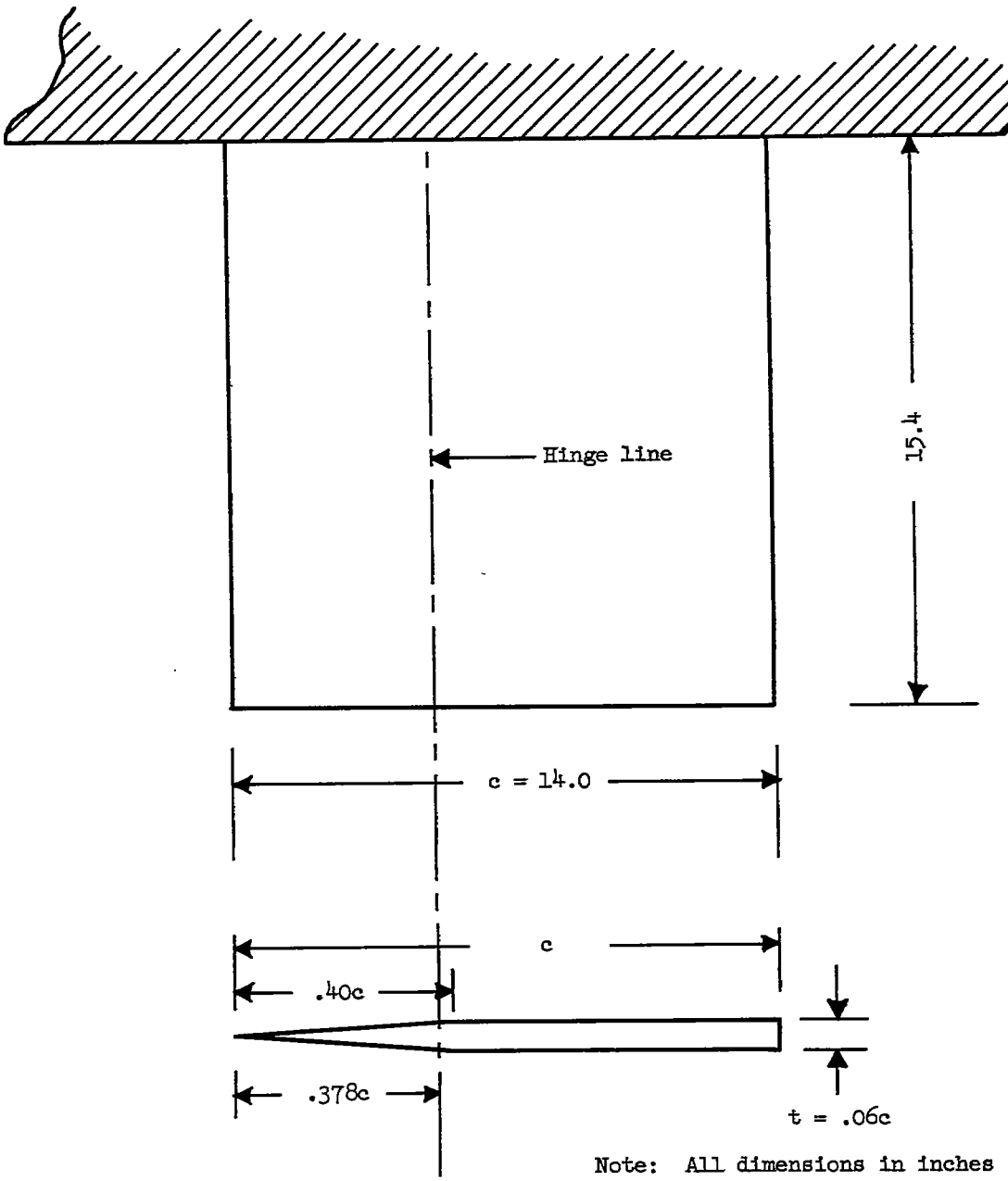

(a) Basic wing.

Figure 18.- Wing- and spoiler-servo description.

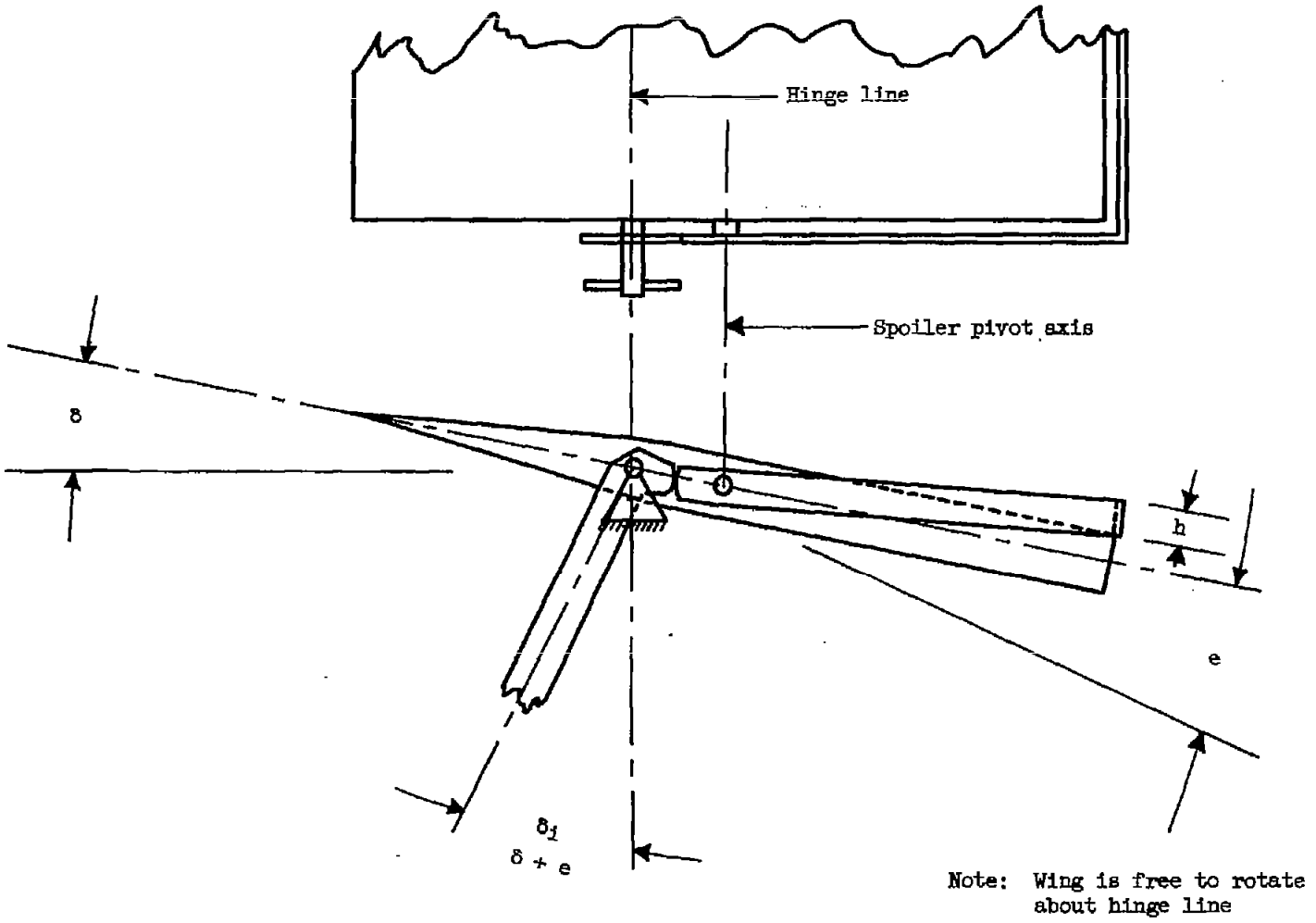

(b) Schematic layout of spoiler servo.

Figure 18.- Concluded.

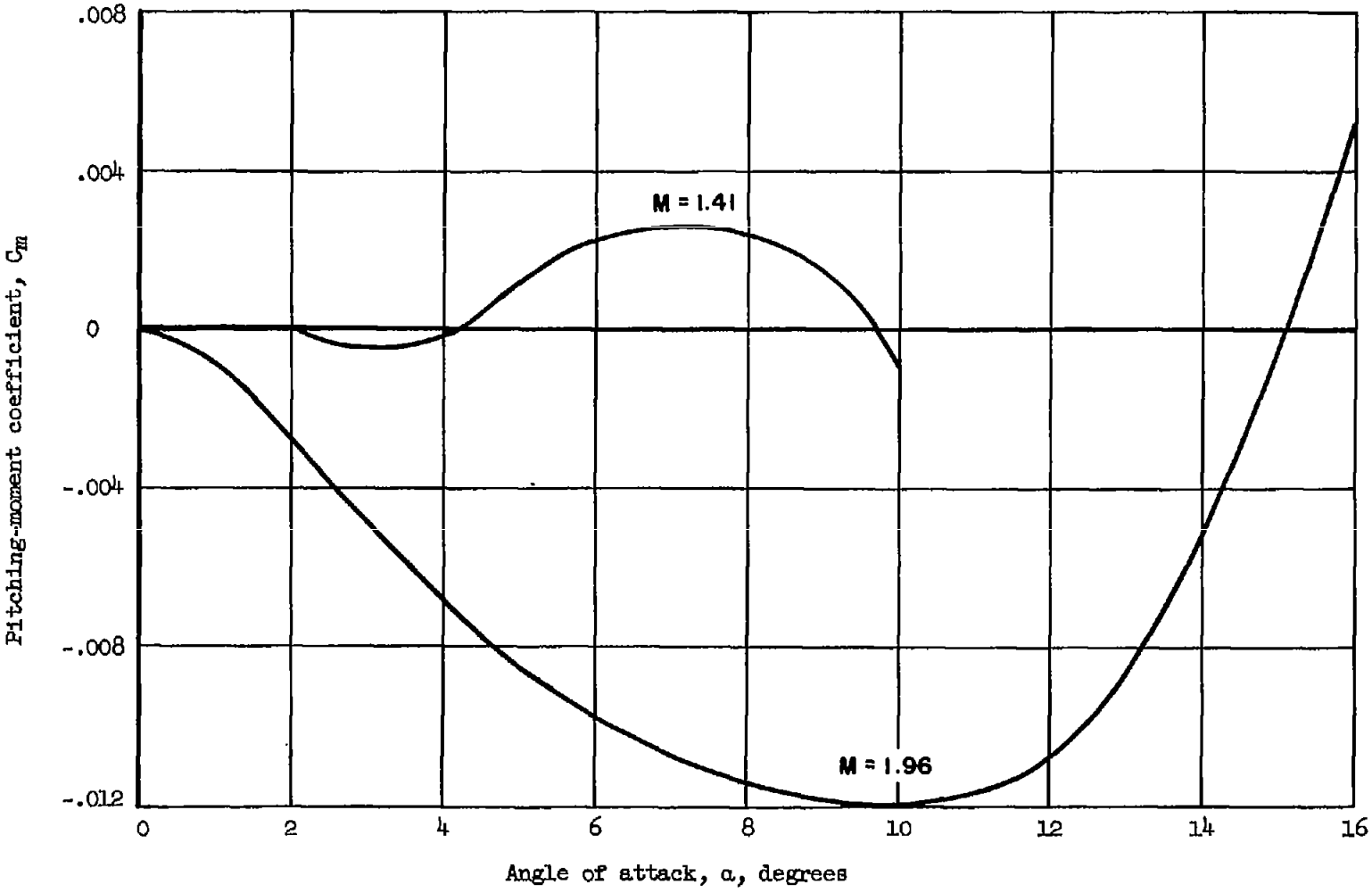

Figure 19.- Pitching-moment characteristics, $C_{m_{0.378\bar{c}}}$.

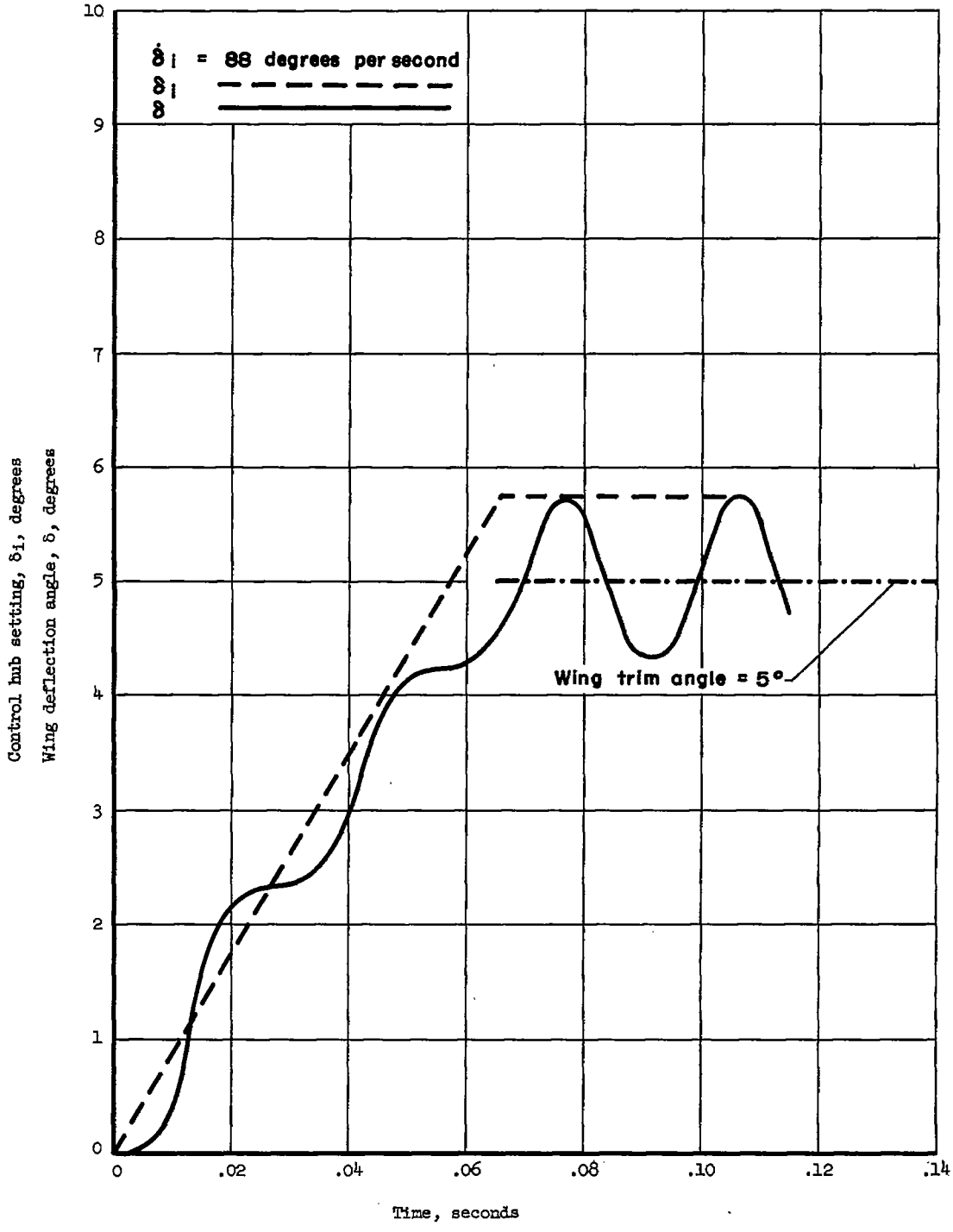

(a) Unbalanced wing.

Figure 20.- Response characteristics of wings.

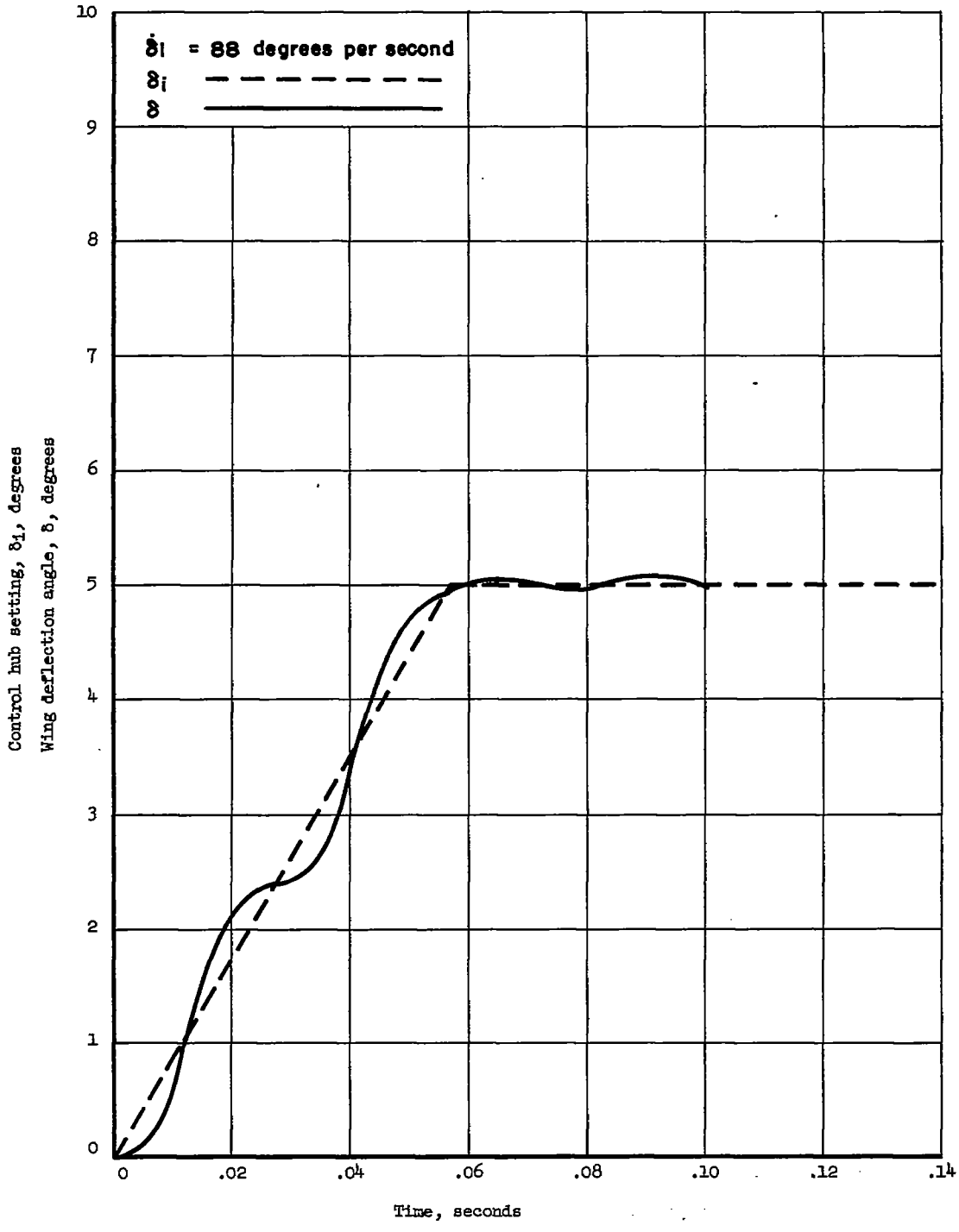

(b) Balanced wing.

Figure 20.- Concluded.

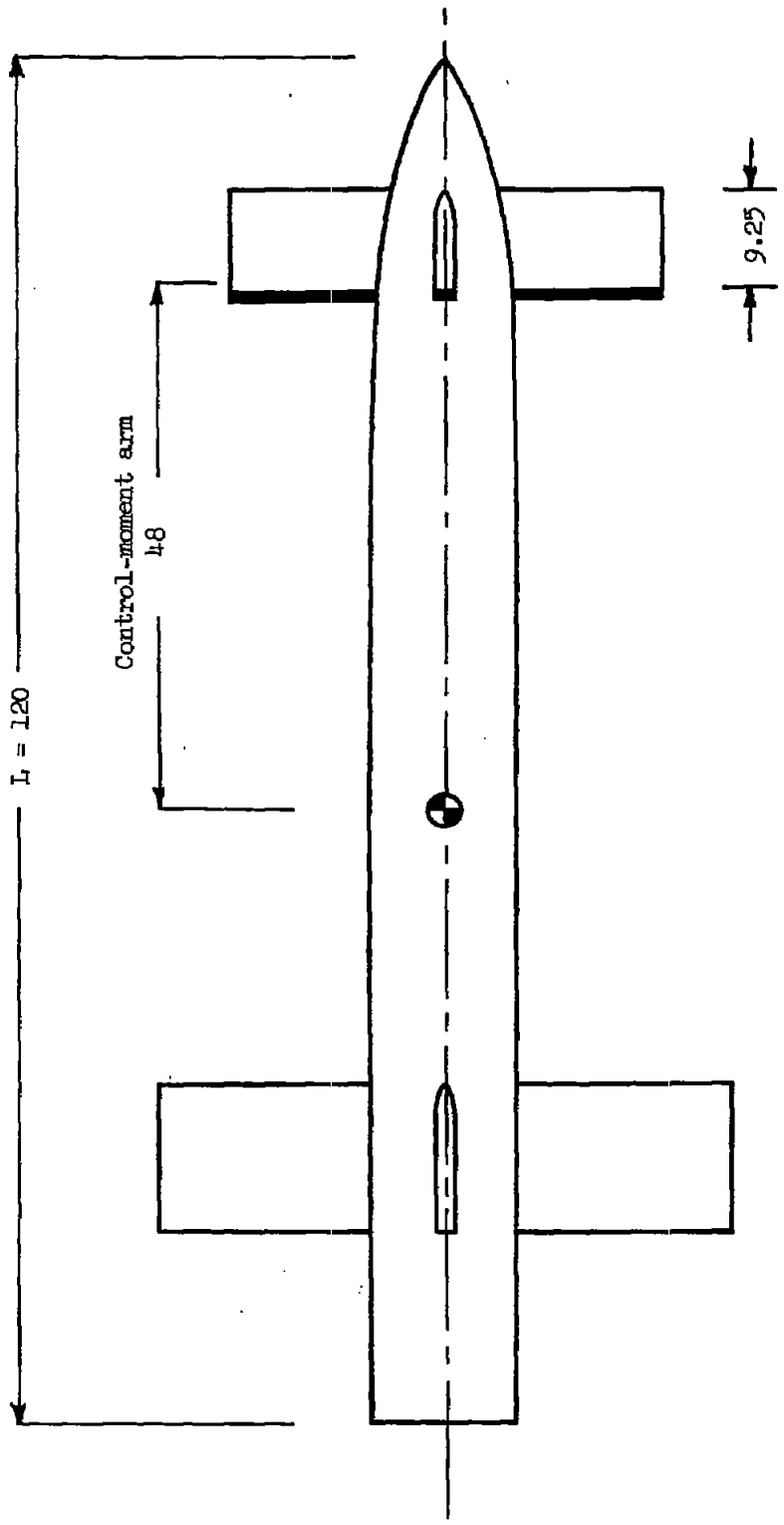

Note: All dimensions in inches

Figure 21.- Sketch of canard missile using spoilers as primary controls.

NACA - Langley Field, Va.